Die approbierte Originalversion dieser Diplom-/Masterarbeit ist an der Hauptbibliothek der Technischen Universität Wien aufgestellt (http://www.ub.tuwien.ac.at).

The approved original version of this diploma or master thesis is available at the main library of the Vienna University of Technology (http://www.ub.tuwien.ac.at/englweb/).

D I P L O M A R B E I T

Palladium micrograins, palladium oxide and silicon oxide in the CO oxidation reaction

Ausgeführt am

Institut für Materialchemie
der Technischen Universität Wien

unter der Anleitung von

Associate Prof. Dipl.-Phys. Dr.rer.nat. Yuri Suchorski

durch

Zuzana Budinská
Mečíková 50
84108 Bratislava, SK

Wien, 2.August 2012

KURZFASSUNG

Das Ziel dieser Arbeit war die Untersuchung der katalytischen CO-Oxidation unter Hochvakuum-Bedingungen mittels *in situ* Photoelektronen-Emissionsmikroskopie (PEEM), Massenspektrometrie (MS) und Röntgenphotoelektronenspektroskopie (XPS). Die CO-Oxidation Reaktion wurde für ihre Bedeutung in der Umweltkatalyse, sowie für den relativ einfachen Langmuir-Hinshelwood Mechanismus, der im Detail auf den Oberflächen von Einkristallen studiert wurde, gewählt. Es ist zu beachten, dass der Einkristall-Ansatz nicht alle Effekte, die bei den üblichen Realkatalysatoren in Wirkung treten, deckt. Das liegt daran, dass die Realkatalysatoren, die hauptsächlich aus Edelmetallpartikeln auf Oxiden bestehen, sich in ihrer Beschaffenheit deutlich von Einkristalloberflächen unterscheiden. In der vorliegenden Arbeit wurden deswegen Modelle gewählt, die sich weiter entlang der "Komplexitätsachse" befinden und besser als die Einkristall-Modelle die Eigenschaften der Realkatalysatoren repräsentieren.

Der erste Schritt weg von den Einkristall-Modellen wurde durch die Untersuchungen der CO-Oxidation auf einer polykristallinen Folie genommen, die aus μm-großen Domänen mit verschiedenen (hkl) Orientierungen besteht. Weiter wurde ein von Aluminiumoxid geträgertes Palladiumpulver als ein raffinierteres Modell verwendet und letztendlich wurde die Reaktion auf einem geträgerten PdO Pulver, mit dem Zweck der Erforschung der Rolle der Oxidphase in der katalytischen CO-Oxidation, untersucht.

Während der Experimenten auf der Palladiumfolie wurde die Bildung einer Oxidschicht, geformt aus den Verunreinigungen, hauptsächlich Silizium, die

aus dem Volumen hinzu der Oberfläche segregieren, untersucht. Die Folie wurde bei erhöhten Temperaturen (400°C - 700°C) mit Sauerstoff (5×10^{-6} mbar) behandelt und nachfolgend wurden die kinetischen Messungen für die CO-Oxidation mittels PEEM und MS, sowie die XPS Untersuchungen der chemischen Zusammensetzung durchgeführt. Die kinetischen Messungen haben eine Abnahme in der Aktivität der katalytischen CO-Oxidation mit steigender Temperatur der oxidierenden Behandlung der Oberfläche gezeigt. Dieser Effekt wurde auf Basis der XPS Messungen erklärt, da die XPS Spektren der oxidierten Probe einen Si 2p Peak, der mit der Oxidationstemperatur wächst, zeigten. Dieser Peak wurde zu höheren Bindungsenergien verschoben gefunden, was auf die Bildung von Silizium-Oxid hinweist. Mit Hilfe eines Arrhenius Plots aus den Si 2p Peakflächen wurde die effektive Aktivierungsenergie für das Segregieren von Si aus dem Volumen und darauf folgende Oxidation bestimmt, diese betrug 0.27 eV. Die beschleunigte Si Segregation in Gegenwart von Sauerstoff kann mit folgenden energetischen Argumenten erklärt werden: die höhere Bindungsenergie von Si auf einer Sauerstoff-bedeckten Pd-Oberfläche bietet eine energetische Senke für Si-Atome aufgrund des chemischen Potentialgradienten und erleichtert somit die Segregation von Si.

Der Einfluss der Probenmorphologie auf die katalytische CO-Oxidation wurde mit Hilfe eines geträgerten Palladiumpulver studiert. Eine solche Probe besteht aus Pd-Partikeln mit vielen Strukturdefekten im Vergleich zu den relativ glatten Domänen der Palladiumfolie. Es wurden kinetische Messungen für die CO-Oxidation durchgeführt und ein globales (mit MS gemessen) sowie ein lokales, ortsaufgelöstes (mit PEEM gemessen) Phasendiagramm wurden konstruiert. Weiterhin wurden "light-off" Experimente unter isobaren Bedingungen durchgeführt und die Ergebnisse (Phasenübergangspunkte) waren in Übereinstimmung mit dem Phasendiagramm, der bei isothermen Bedingungen erstellt wurde. Ein Vergleich der Phasendiagramme für das Palladiumpulver, die Palladiumfolie nach dem Glühen und für die Palladiumfolie nach zusätzlichem Sputtern wurde durchgeführt mit der Schlussfolgerung, dass die defektreichen Oberflächen allgemein toleranter zu der CO-Vergiftung sind.

Auf einem geträgertem PdO Pulver wurde die Rolle von PdO in der katalytischen CO-Oxidation untersucht. PdO hat sich unter den angewendeten Reaktionsbedingungen als instabil erwiesen und war durch Ar^+-Sputtern und Heizen leicht zu reduzieren. Ein Zusammenhang zwischen dem Beitrag des

oxidierten Pd und der Aktivität in der CO-Oxidation wurde festgestellt: der steigende Anteil an PdO in der Probe unterdrückt die katalytische Aktivität bezüglich der CO-Oxidation.

ABSTRACT

The aim of the present thesis was to investigate the catalytic CO oxidation under high vacuum conditions using *in situ* PEEM, MS and XPS techniques. The CO oxidation reaction has been chosen for its significant practical meaning in the pollution control and its relatively simple Langmuir-Hinshelwood reaction mechanism, which has been thoroughly studied on single crystals. However, the single crystals approach does not fully cover all the effects of the real catalysts, consisting of oxide supported precious metal nanoparticles. Therefore, in present thesis different models along the "complexity axis" have been selected, which better represent the properties of real catalysts.

The first step away from the single crystals has been taken by studying the CO oxidation on a polycrystalline palladium foil, which exhibits μm-sized domains of different individual (hkl) orientations. Further an alumina supported palladium powder was used as a more sophisticated model and finally the reaction has also been studied on a supported PdO powder, with the aim to study the role of the oxide phase in the catalytic CO oxidation.

During experiments on the palladium foil the effect of an oxide layer, formed from the impurities which segregated from the bulk, was studied. The foil was treated with oxygen (5×10^{-6} mbar oxygen partial pressure) at elevated temperatures from 400 °C to 700 °C and consequently the kinetic measurements for the CO oxidation with PEEM and MS, as well as the XPS measurements to obtain chemical information have been performed. The kinetic measurements have shown a decrease in the activity towards the catalytic CO oxida-

tion with increasing oxidizing temperatures. This has been explained on the basis of the XPS measurements. The XPS spectra of the oxidized sample have shown a Si 2p peak growing with the increasing oxidizing temperature. This peak has been found as shifted to higher binding energies, which shows the oxidation of silicon. The effective activation energy for the segregation of silicon from bulk and consequent oxide formation has been determined from the Arrhenius plot from the XPS Si 2p peak areas to be 0.27 eV. The enhanced Si segregation in the presence of oxygen can be rationalized considering energetic arguments: the higher bonding strength of Si on an oxygen-covered Pd surface provides an energetic sink for Si atoms due to the chemical potential gradient, facilitating thus the Si segregation.

The influence of the surface morphology on the catalytic CO oxidation was studied on an alumina supported palladium powder. This sample consits of particles with surfaces with many structural defects compared to the domains of a palladium foil. Kinetic measurements were performed and both global and a spatially-resolved local kinetic diagram using MS and PEEM technique respectfully, have been constructed. Additionally "light-off" experiments under isobaric conditions have been carried out and the results were in agreement with the kinetic phase diagram constructed under isothermal conditions. A comparison of the phase diagrams for the palladium powder, palladium foil after annealing and palladium foil after additional sputtering has been carried out with the conclusion, that the defect rich surfaces are more tolerant towards CO poisoning.

The role of PdO in the reaction was studied by performing the CO oxidation on an alumina supported PdO powder. The PdO has proved to be very unstable under the present reaction conditions and easily reduced upon sputtering and heating at elevated temperatures. The correlation between the PdO contribution and the activity in CO oxidation was observed: increasing contribution of PdO in the sample composition suppresses the catalytic activity towards the CO oxidation.

ACKNOWLEDGEMENTS

This Masterthesis would not have been possible without the guidance and help of some individuals, to whom I would like to thank. These people are namely,
my supervisor **Prof. Yuri Suchorski**, who has provided me with motivation, has been willing to answer all my questions during my work and has with much detail and very promptly corrected my thesis,
Dipl.-Phys. Diana Vogel, who has taught me so much in the experimental work in the laboratory and much more about making scientific presentations and writing a thesis, and has been a pleasure to work with,
Dr. rer. tech. Christian Spiel, who has been working in the group at the beginning of my thesis and has introduced me together with Diana to the experimental work,
Martin Datler, who has helped me with some of the measurements,
Johannes Frank, who has done much technical work on the experimental setup,
Prof. Günther Rupprechter, the head of the institute, who has made it possible for me to work on my thesis at IMC,
all the IMC staff, who have created a very friendly and motivating work environment,
FWF (der Wissenschaftsfond), which has provided financial support during my thesis,
my friends and family, with whom I could relax during my free time,
my boyfriend **JB**, who has always listened to me when I complained and was always happy with me, when things were going great,
and finally my parents, **Ivana and Ľuboš Budinskí** , who have always been there for me and provided everything I need for succesfull studies, including their advice and moral support.

TABLE OF CONTENTS

CHAPTER 1

INTRODUCTION

This thesis is dedicated to a surface science study of the catalyzed CO oxidation on palladium and palladium oxide surfaces in high vacuum. In the introduction the roots of research of heterogeneous catalysis are presented. Further on the motivation for studying CO oxidation is discussed and the previous research on this reaction on palladium surfaces is summarized.

1.1 Short history of catalysis

Already in antiquity people have used processes with a catalytic origin, e.g. in the fermentation of sugar to ethanol and in the conversion of ethanol to acetic acid by enzymes. Since this has been done without any understanding of the reaction mechanism, it cannot be spoken of development of catalysis from this period in time [1].

The history of catalysis started with the founders of modern chemistry and physics such as Berzelius, Davy, Faraday, Nernst, Kirchhoff and Ostwald. At the birth of the modern concept stood Berzelius, who, in 1836, was the first to define the term "catalysis" as a process in which certain chemical reactions are facilitated by the presence of substances that remain themselves unaffected [2]. In his time, beginning of the 19th century, the underlying principle of catalysis was still not understood and even later, till the discoveries of Langmuir and Hinshelwood, the scientific work done with the aim of increasing a product rate of a reaction by catalytic materials has been treated close to alchemy.

A modern definition for catalysis which is still valid today has been introduced by Ostwald in 1895: "a catalyst accelerates a chemical reaction without affecting the position of the equilibrium" [3].

Irving Langmuir was the first to study the principles of adsorption and invented the term monolayer. In 1927 the understanding of catalysis took a gigantic step when Hinshelwood presented his kinetic theory based upon early findings of Langmuir. The Langmuir-Hinshelwood mechanism is still used today in modeling of catalytic reactions.

The development of surface science continued in the 1930s with the work of Igor Tamm, who performed ground breaking theoretical work on electron states on metallic surfaces and John Barden, who investigated the electron structure on metallic surfaces. In 1940 Temkin published a detailed description of the kinetics of the ammonia process and Kramer published his study on the kinetics of catalytic reactions. A significant year in the history of catalysis was the year 1950, when the first conference ever, devoted exclusively to heterogeneous catalysis has been held by the Faraday Society. Topics such as adsorption of hydrogen on metals, catalytic activity of silica-aluminum catalysts and electron microscopy and small angle X-ray scattering were presented at this conference. In 1951 Wheeler discovered that diffusion has a significant impact on the activity and selectivity of a catalytic system. First method to characterize catalysts was developed by Eischen and co-workers in 1954. They used IR-spectroscopy to study carbon monoxide adsorption on copper catalyst and also characterized active sites on metal and metal oxide surfaces by adsorption. The first journal devoted solely to catalysis (Journal of Catalysis) was founded in 1962 [4].

Despite of lot of success achieved in the past 150 years in the field of catalysis, the gap between practical catalysis and principal understanding is still large and there is still lot of place for research in this area. With the further development of surface science and computational theoretical chemistry, scientists now have better tools than ever to try to bridge this gap. The main problem still is the difference between model systems in high vacuum conditions used in surface science to explain fundamental principles of catalysis and the nanoparticles used as catalyst in the real high pressure conditions.

The typical surface science approach is to study reactions on single crystals. As illustrated by a "complexity axis" (Fig.1.1), this model is very far from real catalysts. In present work model systems have been chosen which try to simulate some material properties of real catalysts. The reaction has been first studied on a polycrystalline palladium foil, which is the next step along the "complexity axis" from single crystals. The polycristalline foil consists of many micrograins with different crystallographic orientations, with grain boundaries between them and defect sites. The corresponding results are presented in chapter 3. The next step which has been done in the present work is a step from the micrograins of a polycrystalline palladium foil to a palladium powder pressed onto an

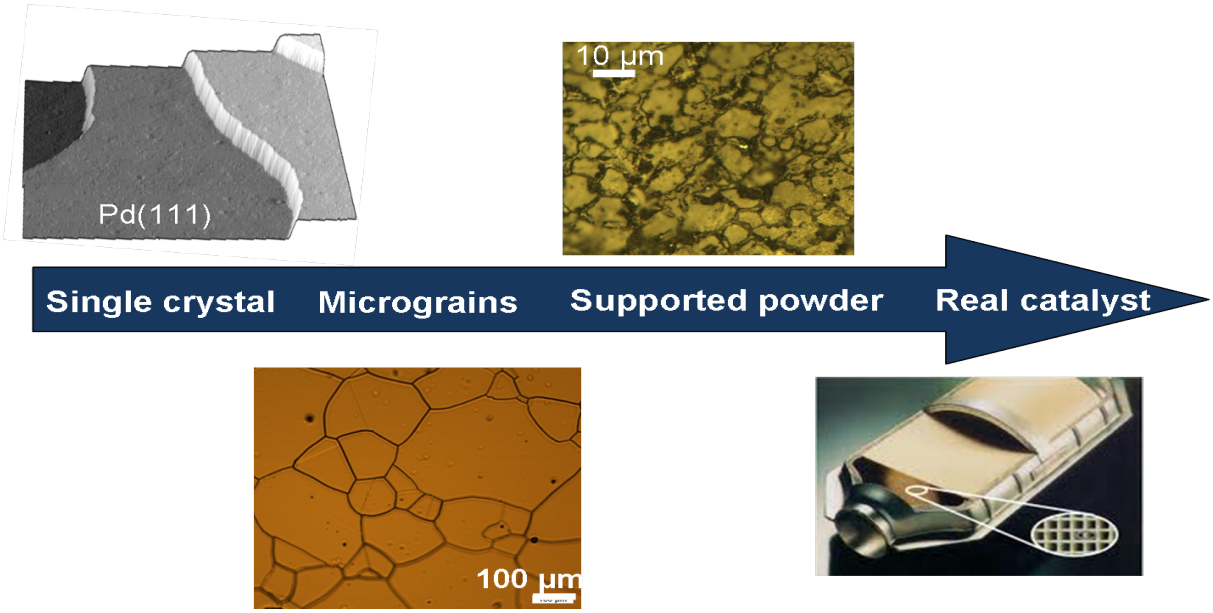

Fig. 1.1: Illustration of "complexity axis", model systems in surface science.

alumina support (chapter 4). The third model system on which experiments have been performed in this work is palladium oxide powder on an alumina support (chapter 4).

1.2 Principles of catalysis

Each chemical reaction involves breaking of bonds between atoms and the formation of new ones. In the energy diagram (Fig. 1.2) the energies for the reaction $A + B \longrightarrow C$ are represented. The reaction rate constant for this reaction can be expressed by the Arrhenius equation:

$$k = Ae^{-\frac{E_a}{k_B T}} \tag{1.1}$$

where k is the reaction rate constant, E_a is the activation energy,A is the pre-exponential factor, k_B is the Boltzmann constant, and T is the temperature. An increase in the reaction rate can be achieved either by increasing the temperature or by lowering the activation energy. The later can be achieved by the means of a catalyst, which forms intermediate compounds, thus creating an alternative reaction path with a lower energy barrier to overcome, shown in the diagram as the dotted line (Fig.1.2). If the educts and catalyst are in the same phase, the process is called homogeneous catalysis, and in the case of a catalyst in a different phase (most commonly educts in gaseous or liquid phase and a solid phase

catalyst) the process is called heterogeneous catalysis. In the later case, some or all of the reacting species are adsorbed on the catalyst surface before the reaction takes place. The atoms in the surface layer of solids have fewer neighbors than those in the bulk and hence may form new bonds with atoms or molecules by chemisorption. During adsorption, the existing bonds may be modified or even broken, as in the case of a dissociative adsorption. The adsorbed species may also diffuse towards each other and react. The formed product leaves the surface by desorption.

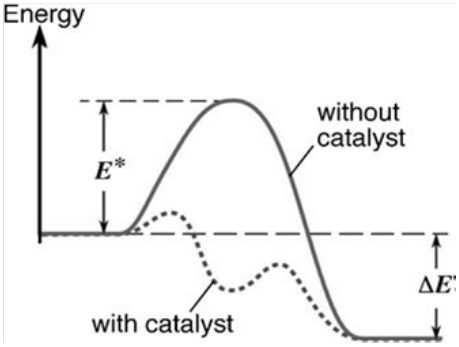

Fig. 1.2: Energy diagram for reaction with and without catalyst [5].

1.3 Palladium

The precious metal that has been used in the samples studied throughout this thesis is palladium. This element has the atomic number 46 and the electronic configuration $1s^2 2s^2 2p^6 3s^2 3p^6 3d^{10} 4s^2 4p^6 4d^{10}$. It belongs to the platinum group metals, has a silvery-white color and crystallizes in the face centered cubic crystal lattice. The planes of a palladium unit cell with the Miller indices (111), (100) and (110) are shown in the figure 1.3.

The crystallographic orientation plays an important part in the surface properties in general and in the CO oxidation reaction in particular. As shown in the Fig.1.3, different (hkl) planes have a different density of atoms and thus also different adsorption sites. As the catalytical CO oxidation takes place only when both educts are adsorbed on the surface, this is an important factor. The density of atoms on the surface also influences, as will be explained later on, the electron density near the surface and thus the work function of the surface. The most densely packed is the (111) plane and the least densely packed is the (110). The work function for Pd(111) is 5.95 eV, for Pd(100) 5.65 eV and for Pd(110) 5.20 eV [7].

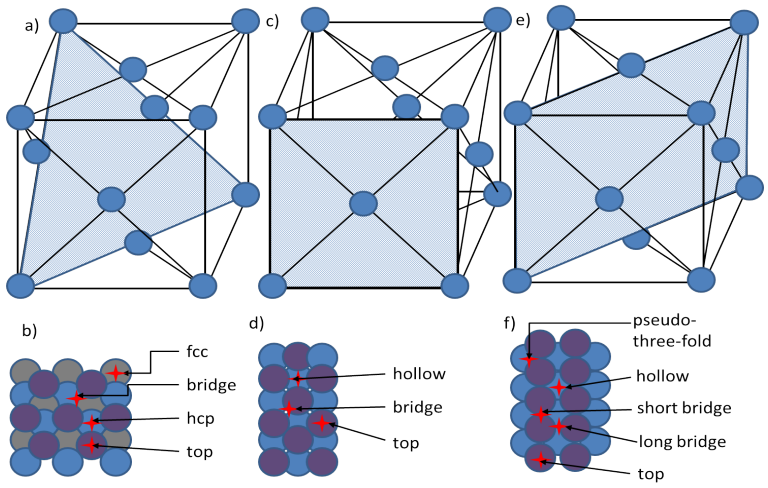

Fig. 1.3: a) Pd(111) plane; b) schematic representations of adsorption sites on Pd(111) plane: fcc, bridge, hcp, top; c) Pd(100) plane; d) schematic representations of adsorption sites on Pd(100) plane: hollow, bridge, top; e) Pd(110)plane; e) schematic representations of adsorption sites on Pd(110) plane: pseudo-three-fold, short bridge, long bridge, hollow, top. Adapted from [6].

1.4 Alumina as support

In the first part of the introduction the need of a model which mimics the real catalyst was mentioned. In present work results of measurements for a palladium powder brought onto an alumina support are also presented. Therefore, the role of the alumina as a support for catallytically active material is explained in this section.

Metal nanoparticles are often unstable and tend to sintering at higher temperatures. The stabilization of these particles can be done by so-called structural promoters or by applying the particles inside the pores of an inert support. Alumina has excellent thermal and mechanical stability, it exists in various structures, however only three are of interest for the catalytic application. These are the nonporous, crystallographically ordered $\alpha-Al_2O_3$, and the porous and amorphous η - and γ- Al_2O_3. The later can also be used as a catalyst, e.g. in the production of sulfur or alkylation of phenol. In present work an oxidized aluminum foil was used as support.

1.5 CO oxidation reaction

Carbon monoxide is a poisonous gas and its elimination from the atmosphere is crucial. Therefore the oxidation of CO to far less harmful CO_2 is an important subject that needs to be dealt with. Besides its importance in environmental chemistry, the CO oxidation plays

an important role in fuel cell technology, namely in the PEM (Proton Exchange Membrane) fuel cells CO has to be completely removed, since it acts as a severe catalyst poison [8].

1.5.1 Environmental importance

In the recent years lot of public attention has been turned to environmental problems. The negative impact of the exhaust gases from automobile engines was debated heavily already in the late 1960s. In 1990 the total number of cars, trucks, buses and motorcycles in the world was estimated to be about 650 million and this number is growing every year. All these vehicles produce exhaust gases, consisting of N_2, water vapor, CO, hydrocarbons and nitrogen oxides and it is estimated that 500 000 people per year die as a result of transportation-related air pollution.

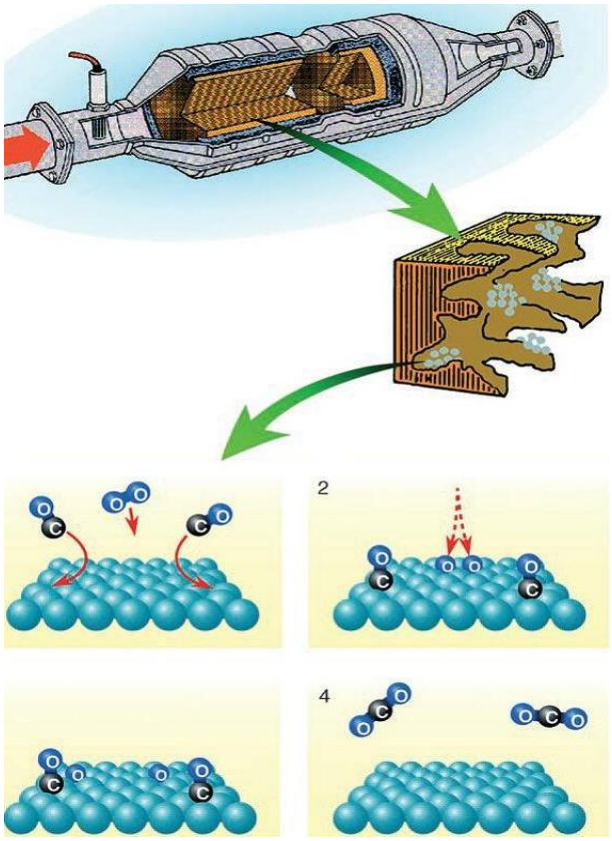

Fig. 1.4: Schematic illustration of TWC and the mechanism of CO oxidation [5].

The first commercial exhaust after-treatment system where CO was oxidized to CO_2 was developed by Engelhard [4]. Today cars use a so called TWC, three-way catalytic converter, which not only converts poisonous CO to less harmful CO_2, but also oxidizes

unburned hydrocarbons and reduces oxides of nitrogen. Such a converter consists of a ceramic monolith with a honeycomb structure to provide high surface area for the washcoat, the washcoat itself, and noble metal particles, which are the actual catalysts in the system (Fig. 1.4). Alternatively to ceramic, a metallic foil monolith from FeCrAl can be used, which is less expensive in small production quantities. The washcoat serves as the carrier for the catalytic material. Aluminum oxide, titanium dioxide, silicon dioxide or a mixture of the previous are typical washcoat materials. Alumina is used in its gamma modification and has the most suitable high surface area needed for the support of noble metals (surface are of 150 - 175 m^2/g [9]). However at high temperatures gamma alumina changes its modification into the alpha phase, which needs to be prevented. Another disadvantage lies in the diffusion of noble metals, mainly Rh, into alumina.

The catalyst itself is a precious metal present as dispersed nanoparticles on the washcoat. Platinum can be used for both reduction and oxidation, is the most active, but not suitable for all applications due to unwanted reactions and high cost. It is relatively insensitive to contamination by lead or sulfur. At higher temperatures it may come to sintering of the nanoparticles, leading to a decrease in the surface area of platinum and consequently to deactivation. Rhodium is often used as a reduction catalyst. It is very expensive, but has unique surface properties with respect to NO surface chemistry. Palladium can be present in addition to rhodium and platinum, but may also replace them fully. Palladium is good for oxidation of both CO and hydrocarbons, but is somewhat less active towards the reduction of NO. Hence catalyst consisting of only palladium may have 5 - 10 times higher loading than a Pt-Rh catalyst. Other metals in use are cerium, iron, manganese and nickel.

The ideal temperatures for operating a TWC lie between 350 and 650 °C. Since it takes some time for the converter to reach this temperature after starting the engine, most of the CO and hydrocarbons emission takes place before. Temperatures above 800 °C should be avoided to prevent sintering of noble metal particles together and the diffusion of rhodium, if used, into the alumina washcoat.

1.5.2 Mechanism of the CO oxidation reaction on platinum group metals

The CO oxidation is often the reaction of choice for many catalysis research groups, not only because of its importance in the environmental chemistry as already discussed, but also because it follows a rather simple microscopic reaction mechanism. As Engel and Ertl

proved in 1978, the CO oxidation on palladium obeys the Langmuir-Hinshelwood mechanism, meaning that the reaction takes place between both reactants in their chemisorbed state [10]. The steps of the Langmuir-Hinshelwood mechanism are as follows:

$$CO + * \rightleftharpoons CO_{ad}$$

$$O_2 + 2* \rightleftharpoons O_{2,ad} \rightharpoonup 2O_{ad}$$

$$CO_{ad} + O_{ad} \rightharpoonup CO_2 \uparrow + 2*$$

First step is the adsorption of CO and O_2 on the metal surface. A free site is indicated by *. Oxygen undergoes a dissociative adsorption, where both adsorption sites do not differ from each other. On the other hand, CO adsorbs molecularly to the metal. The desorption of oxygen needs higher temperatures, than CO desorption. In the next step of the Langmuir-Hinshelwood mechanism the adsorbed CO and adsorbed O react together and at temperatures, at which the reaction occurs, CO_2 can immediately be desorbed from the surface as the product.

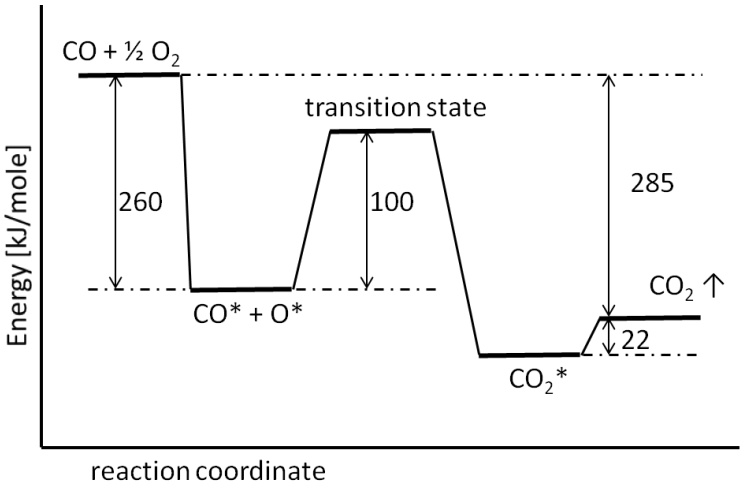

Fig. 1.5: Approximate energy diagram of CO oxidation on palladium [10].

The activation energy of the homogeneous gas-phase reaction between CO and oxygen is largely determined to be 500 kJ/mole. This energy is needed to break the O-O bond of oxygen and hence the dissociation of oxygen is in this reaction the rate-determining step. This is where the catalysts come into play, by easily dissociating the oxygen molecule. In the case of a catalyzed CO oxidation reaction on Pt-group metals the rate-determining step is the recombination of adsorbed oxygen and adsorbed CO to give adsorbed CO_2, which has an activation energy of about 100 kJ/mole, thus 5 times lower than reaction

without a catalyst. This is the largest energy barrier that needs to be overcome in a catalyzed CO oxidation, hence it is the rate-determining step of the reaction (Fig. 1.5).

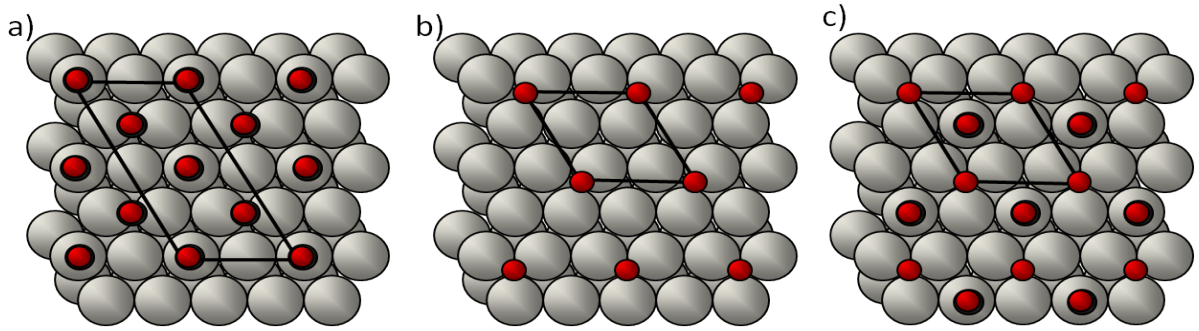

Fig. 1.6: a) Adsorption of CO on Pt(111); the c(4×2) saturated coverage leads to inhibition of dissociative adsorption of oxygen and thus deactivation of the catalyst surface. b) Adsorption of O on Pt(111) leading to a p(2×2) O - structure. c) CO adsorption on the O - covered surface as shown in (b), reaction can take place. Based on [11, 12].

Depending on the temperature of the catalyst and on the partial pressures of CO and O_2 in the gasphase, the surface of the metal can either be oxygen- or CO-covered. These surfaces differ dramatically from each other in the catalytic activity. At low temperatures the surface is predominantly covered by CO. Above the desorption temperature of CO, oxygen can build up on the surface, provided the partial pressure of oxygen is high enough. The reason for the different activity of both surfaces lies in the different adsorption mechanism of CO and oxygen (Fig. 1.6). CO adsorbs molecularly to the surface and forms a dense coverage on the metal (Fig.1.6a). On the other hand oxygen undergoes a dissociative adsorption and needs two free adsorption sites next to each other, which are not present on a CO-covered surface. Since oxygen can hardly adsorb on a CO-covered surface, such surface is catalytically inactive and is referred to as CO poisoned. Adsorbed oxygen forms a less dense coverage (Fig.1.6 b), so that CO, which needs only one free site for its molecular adsorption, can coadsorb on an already oxygen-covered surface (Fig.1.6 c) and the CO oxidation reaction can occur.

As already mentioned, the state of the catalyst can be controlled by extern control parameters, such as the temperature and partial pressures of CO and O_2. In present thesis experiments have been carried out mainly at constant oxygen pressure and temperature and under variation of CO pressure, which leads to either an oxygen-covered surface for relative low CO pressures or a CO-covered surface for relative high CO pressures.

Beginning with an oxygen-covered surface, the reaction rate increases approximately linearly with increasing CO pressure till a kinetic transition point τ_A is achieved, where

this steady state is suddenly changed to the state where the surface is CO-covered. This state, as already explained, is inactive for the CO oxidation and thus an abrupt decrease in the reaction rate is observed (Fig. 1.7). When the CO pressure is lowered, the second kinetic transition τ_B, i.e. transition from the CO-covered to the oxygen-covered surface, can be observed. This kinetic transition is characterized by the sudden increase in reaction rate and occurs at a lower CO pressure than τ_A, thus showing a hysteresis behavior.

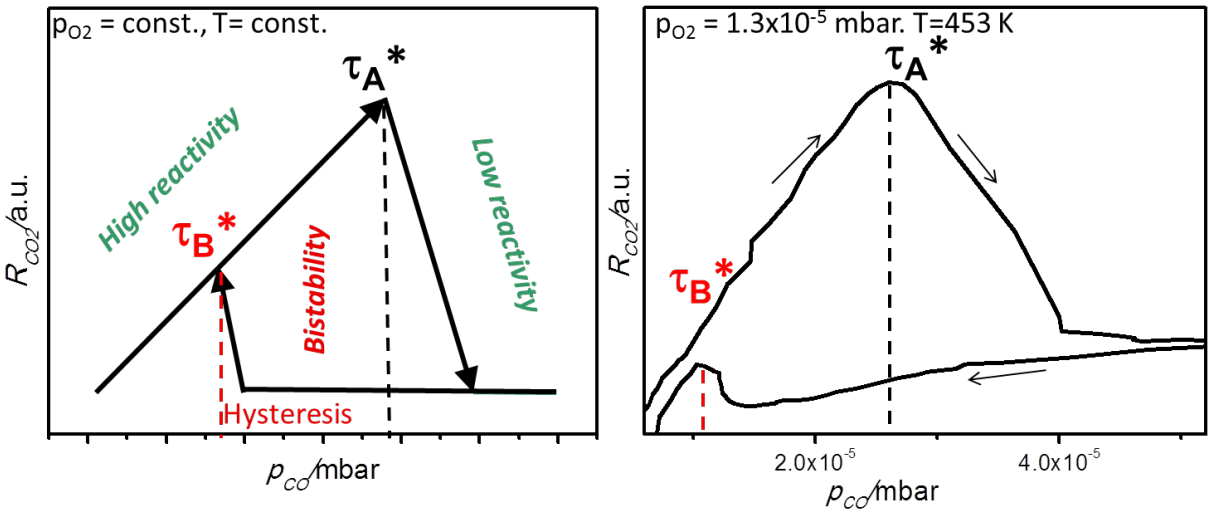

Fig. 1.7: Left: schematic hysteresis in the CO_2 rate for constant oxygen pressure and temperature shown as a function of CO pressure. Right: An experimental hysteresis curve: the CO oxidation on Pd powder at constant temperature (T= 453 K) and oxygen pressure (p_{O_2}=1.3×10^{-5} mbar) .

Between τ_A and τ_B the system is bistable, meaning there is a set of control parameters under which the catalyst can find itself in either one of the steady states, oxygen- or CO-covered. Whether the system finds itself in one or the other steady state is only a question of how the bistability region has been reached.

The series of such isothermal hysteresis loops can be summarized in a so called reactive kinetic phase diagram, i.e. a plot of the kinetic transition points, τ_A and τ_B, as a function of reciprokal temperature. At a certain high temperature the bistability region becomes infinitely small and achieves a cusp point (Fig. 1.8).

The term "phase diagram" for the description of kinetic transitions from active to inactive states is justified by the analogy to equilibrium thermodynamics and has already been used by F. Schlögl in the seventies [13–15]. The appearance of instabilities or kinetic oscillations in the CO oxidation reaction on Pd surfaces is related from this point of view to the appearance of different competitive reactive "phases". Such phase diagrams have been successfully used for revealing mechanisms of bistability and oscillations for reac-

tions in homogeneous phase such as the Briggs-Rauscher or Belousov-Zhabotinsky oscillating reactions [16, 17] and are applied also to heterogeneous systems since more than one decade ago. The phase diagrams of the CO oxidation have a characteristic triangular-like shape and are therefore often referred to as cross-shaped phase diagrams [18] or (because of the branching at the transition points) as bifurcation diagrams [19].

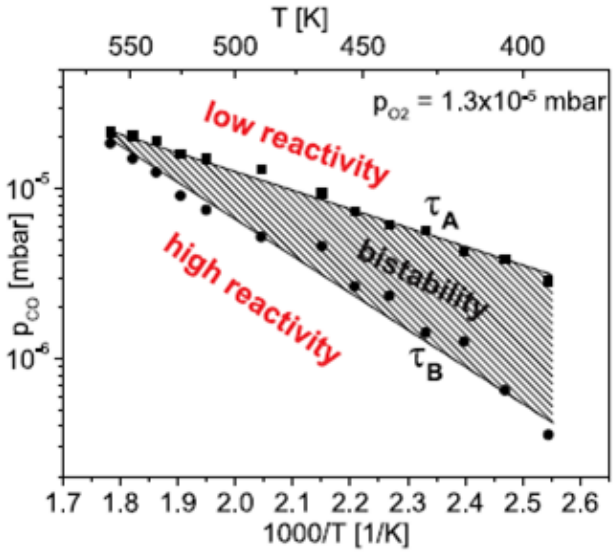

Fig. 1.8: Global kinetic phase diagram for a polycrystalline Pt foil for constant p_{O_2}=1.3×10^{-5} mbar and temperature in the range from 393 to 593 K. The bistability region is indicated by a diagonal line pattern [20].

CHAPTER 2

EXPERIMENTAL

This chapter describes the ultra-high vacuum setup used for the experiments in present thesis and also explains the working principles of the used surface science techniques, namely photoemission electron microscopy (PEEM), mass spectrometry (MS) and X-ray photoelectron spectroscopy (XPS).

2.1 Experimental setup

All experiments were performed in an UHV setup, named HELIOS, consisting of two separate chambers which are connected by sample transfer system with a load lock. This setup, shown in Fig. 2.1 gives the possibility to study reactions using PEEM, MS, LEED and XPS techniques. The transfer system allows transfer of the sample from a chamber with PEEM, LEED and MS arrangement ("PEEM chamber") to a chamber with the XPS technique ("XPS chamber") directly after performing kinetic measurements and even, if so wished, allows to keep the sample after transfer and during the XPS measurements under the same atmosphere. The load lock between the chambers has a parking space and allows the sample to be taken out of the system without breaking the vacuum in the measurement chambers.

During the experiments it is necessary to have a sample surface free of contaminations and also ensure a sufficient mean free path of electrons, emitted during PEEM and XPS measurements. For this purpose UHV is necessary, which is achieved by a series of vacuum pumps connected to the chambers.

The UHV "PEEM chamber" (Fig. 2.1) is being evacuated by an ion getter pump (Vaclon Plus 500,Varian), a titanium sublimation pump (TSP, Varian), and a large turbomolecular

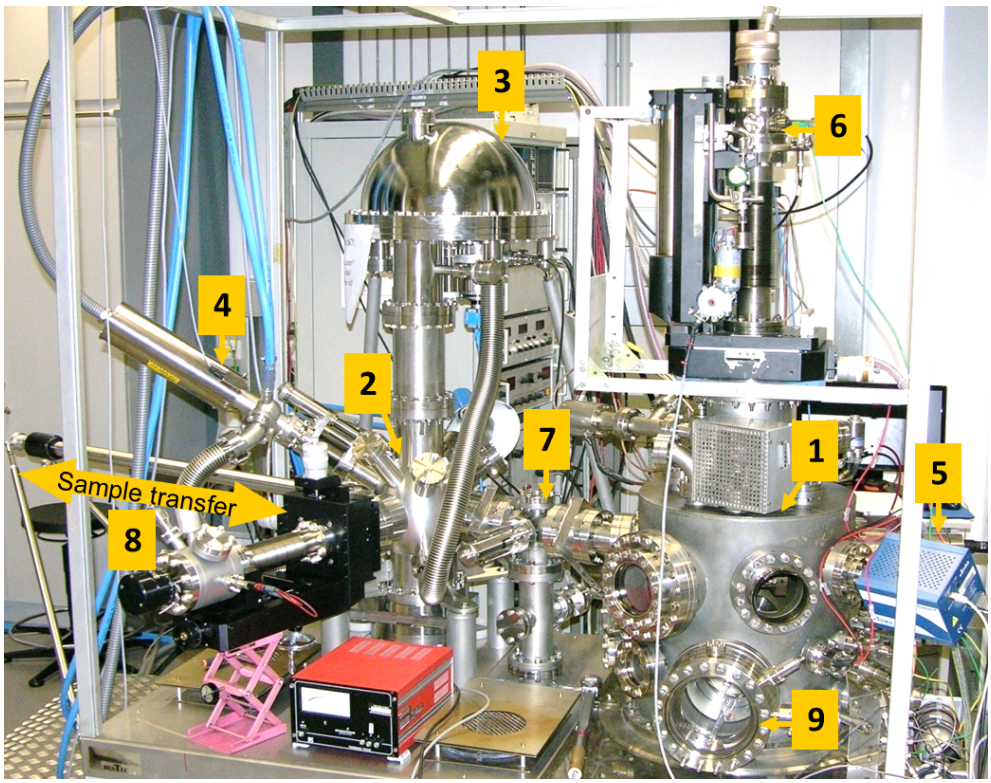

Fig. 2.1: UHV system "Helios" with 1) "PEEM chamber" equipped by PEEM, LEED and MS evacuated by ion getter pump, titanium sublimation pump and two turbomolecular pumps, 2) "XPS chamber" containing XPS technique, evacuated by ion getter pump, 3) XPS hemispherical analyzer, 4) X-ray source used for XPS measurements with Mg and Al anode, 5) MS, 6) manipulator for moving the sample within the "PEEM chamber", 7) load lock connecting the "PEEM chamber" and the "XPS chamber", evacuated by a turbomolecular pump, 8) transfer rod used for transport of the sample between the two chambers 9) LEED, which has not been used in present work.

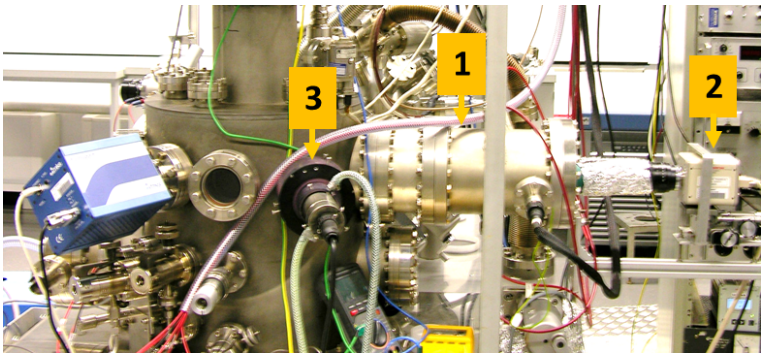

Fig. 2.2: UHV system "Helios" side view with 1) PEEM 2) high speed CCD camera 3)Deuterium UV lamp used as UV light source during PEEM measurements.

pump (TMU 260, Balzers) connected to a rotary vane pump (TriVac D8B, Leybold). Since the PEEM technique is in a need of a pressure lower than 10^{-5} mbar, the space directly in front of PEEM can be differentially pumped out by an additional small turbomolecular pump (TMU 071P, Pffeifer Vacuum) during experiments with pressure up to 10^{-4} mbar. The load lock is being evacuated by a turbomolecular pump (HiPace 80, Pffeifer Vacuum) connected to a rotary vane pump (Duo 5, Pffeifer Vacuum). The "XPS chamber" is pumped by an ion pump (StarCell 300, Varian).

The pressure measurement devices installed for use in "PEEM chamber" are a Bayard-Alpert hot cathode ionization gauge (Varian) and spinning rotor gauge (Viscovac, Leybold). It is important to monitor the total pressure in the chamber, but also partial pressure of reaction gases for kinetic measurements. Partial pressures are measured by MS. During differential pumping in front of PEEM, Viscovac is used to measure the reaction pressure in the chamber. The "XPS chamber" and load lock are monitored by a thermal conductivity Pirani gauge (ThermoVac, Leybold). For pre-vacuum a Thermovac (TM 230, Leybold) is used.

Before each experiment, the surface of the sample should be cleaned. Usual method for obtaining an atomically clean surfaces in UHV is Ar^+ ion sputtering and consequent annealing. In this experimental setup sputter gun (IQE 11/35, SPECS) is used, and Argon (99.999%,Messer) is dosed from a 1 L MINICAN through a leak valve. For annealing of the sputtered surface a thoriated tungsten filament is positioned behind the sample and allows the sample to be heated by indirect radiation. If higher temperatures (more than ca. 700 K) are necessary, the same filament can be used for the electron bombardment of the sample. The temperature can be measured by a type K (Chromel/Alumel) thermocouple spot-welded directly to the sample and additionally by an external movable thermocouple which can be brought to contact with the sample at any point of its surface and has been used primary for calibration and control of the thermocouple fixed on the sample.

The photoelectron emission microscope used in this work is a PEEM 150 (STAIB Instruments) and is described in chapter 2.2. For kinetic reaction measurements a quadrupole mass spectrometer (e-$Vision^+$, MKS Instruments) is installed at "PEEM chamber" (chapter 2.3). The "XPS chamber" is equipped with an X-ray source (XR 50, SPECS) and a hemispherical electron energy analyzer (Phoibos 100, SPECS) for XPS measurements (chapter 2.4).

The reaction gases oxygen and carbon monoxide are dosed into the "PEEM chamber" by leak valves. Gases of high purity (O2: 99.999%, Messer; CO:99.97%, Linde) stored in 1 L MINICAN bottles were used.

Within the "PEEM chamber" the sample can be rotated in 360° and moved in x-,y- and z-axis by a manipulator. This way the sample can be moved from a position facing the sputter gun to the "PEEM position" or to a window for observation.

2.2 Photoemission electron microscopy

One of the main techniques used in the present work is the photoelectron emission microscopy (PEEM). It is used for imaging of the sample surface, monitoring of the *in situ* reaction and for the local kinetic measurements.

The first working photoemission electron microscope was built by Brüche in 1932 using ultraviolet (UV) light source to image a metal surface by the UV-light excited photoelectrons [21]. The principal design of this PEEM is still used today.

The first commercially available PEEM was designed and tested by Engel during the 1960s for his thesis work under supervision of E. Ruska. It was developed into a marketable product called the "Metioskop KE3" by Balzers in 1971. The electron lenses and voltage divider of the PEEM were incorporated into one version of a PEEM for biological studies in Eugene, Oregon around 1970. In the 80s and 90s G. Rempfer, E. Bauer, G. Schönhense, and B. Tonner besides others developed improved electron optics , which are in principle similar to the optics of Low Energy Electron Microscopes (LEEM). This allowed the improvement of the spatial resolution, which can today achieve even 10 nm by the use of synchroton radiation.

The main principle of PEEM lies in the photoelectric effect, known since its discovery by Hertz [22] and Hallwachs [23] in 1887. When electromagnetic radiation of short wavelength, such as UV-light or X-ray interacts with a solid state sample, electrons can be emitted from the surface as a result. These electrons are then called photoelectrons. Einstein‘s law for the photoeffect is formulated by the following equation [24] (Nobel Prize in 1922) :

$$E_{kin} = h\nu - E_B - \Phi_S \tag{2.1}$$

Here Φ_S is the work function of the sample, hν is the energy of the UV (or X-ray) photon, E_B is the characteristic binding energy of the emitted photoelectron and E_{kin} is the kinetic energy of the emitted photoelectron. In PEEM, mainly UV radiation (energies between 3 and 124 eV) is taken as an excitation source. The UV radiation is able to excite valence electrons, but not the core electrons of an atom. For the emission of the core electrons, the X-ray excitation is necessary.

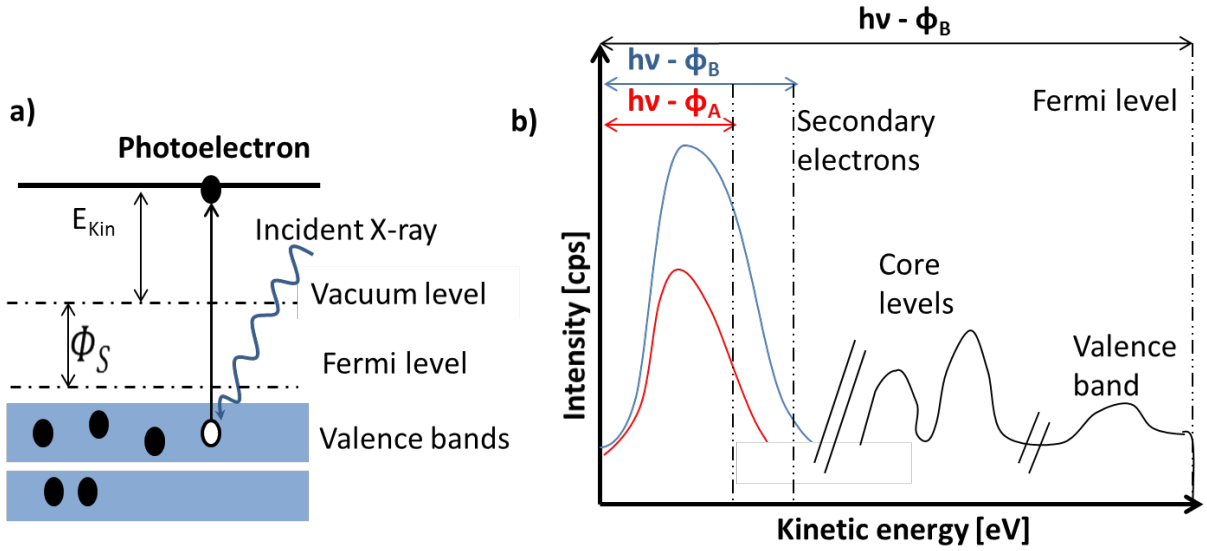

Fig. 2.3: a) Energy level diagram of the photoelectic effect: the work function is the energy difference between the Fermi level and the vacuum level and the kinetic energy E_{kin} of the emitted photoelectrons obeys the Einstein's equation. b) Schematic resulting photoemission spectrum for two different work function values $\Phi_A > \Phi_B$. In the case of UV light excitation, core level peaks are not available.

The work function is defined as the energy necessary to extract an electron from the Fermi level to vacuum level. The work function varies for different elements, and depends also on the crystallographic orientations, local variations in surface topography and presence of adsorbates on the surface. In this way, local emission of photoelectrons and thus the contrast of the PEEM image is dependent on the local work function. The majority of the emitted photoelectrons are the inelastically scattered secondary electrons with low kinetic energy, which are rather useless and disturbing for spectroscopic techniques. These secondary electrons are valuable for PEEM, since a large number of electrons is necessary to create sufficient intensity. The value of the local work function Φ also has a major influence on the local photoemission intensity, as is shown in Fig. 2.3.b for two different work function values Φ_A and Φ_B ($\Phi_A > \Phi_B$). An example for the whole spectrum, which is here shown only schematically can be seen in Fig. 2.9.

In the Fig. 2.4 a PEEM image of a polycrystalline palladium foil is shown. The contrast of the image is caused by the crystallographic orientations, but also by presence of different adsorbates. The darkest grain on this picture is the one with (111) crystallographic orientation. This observation is in correlation with the cognition, that the crystallographic plane with higher atomic density also has the higher work function, which is, according

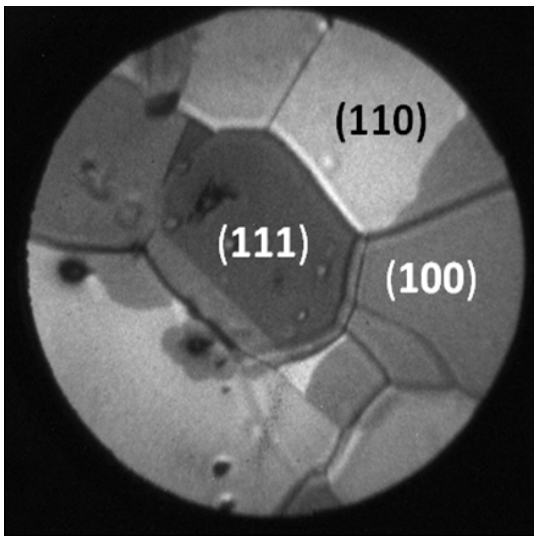

Fig. 2.4: Example of a PEEM image of a palladium foil.

to Smoluchowski's theorem, caused by the redistribution of the electron cloud on a metal surface with varying corrugation [25].

In this way, grain boundaries and defect sites can also be seen by PEEM. The difference in the intensity within one grain may be caused by different adsorbates. The image in Fig. 2.4 has been taken during a CO oxidation reaction, so a transition of the Pd surface from oxygen-covered to CO-covered is portrayed *in situ*. When one compares the clean Pd surface, the oxygen-covered and the CO-covered surfaces, the clean surface has the lowest work function, thus the highest PEEM intensity, meaning that the brightest image is the image of a clean palladium. An oxygen-covered surface is brighter than the CO-covered, which has the highest work function. Not all adsorbates cause a change in the work function. The commonly accepted observation is that electronegative adsorbates increase the work function of the surface, however there are few exceptions known.

The STAIB-PEEM as it has been used for present measurements is illustrated schematically in the Fig. 2.5. The voltages which were applied in present measurements are as follows: 15 kV transfer voltage, 2-4 kV on the objective lens, ca.10 kV on the intermediate lens, 1.58 kV on the projective lens, 1.25 kV on the decel lens, 0.750 kV on the micro-channel plate and 3 kV on the phosphor screen. The objective lens is used for focusing and the intermediate lens for magnification of the image. The image created by photo-electrons on the phosphor screen can be monitored by a high-speed CCD camera (Hamamatsu, C9300). The UV radiation for the working of PEEM is provided by a deuterium discharge UV lamp (D200, Heraeus, Germany).

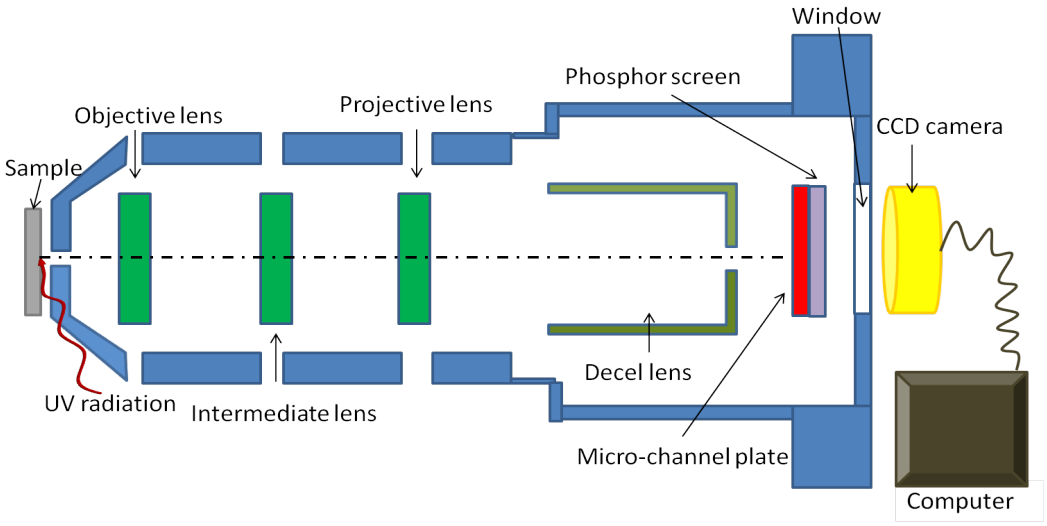

Fig. 2.5: Schematic illustration of PEEM from STAIB Instruments.

2.3 Quadrupole mass spectrometry

For the kinetic measurements a technique, which can measure the reaction product rate is needed. Quadrupole mass spectrometry can selectively measure the partial pressure of all gas components including CO_2, the product of the CO oxidation reaction.

A mass spectrometer usually measures the mass-to-charge ratio of ionized gas particles, after the neutral gas molecules or atoms are ionized by interacting with accelerated electrons. To the largest extent single positively ions M^+ are created, apart of a small part of higher charged ions and charged fragments. These ions are accelerated by an electric field towards the mass-to-charge analyzer. The analyzer separates the ions according to their mass-to-charge ratio (m/z). The separation occurs usually by a magnetic field, i.e. the Lorentz force (2.2) and Newton's second law of motion (2.3) can be combined:

$$\boldsymbol{F} = Q(\boldsymbol{E} + \boldsymbol{v} \times \boldsymbol{B}) \tag{2.2}$$

$$\boldsymbol{F} = m\boldsymbol{a} \tag{2.3}$$

where $\boldsymbol{F}$ is the force applied to the ion, Q is the ion charge, $\boldsymbol{v} \times \boldsymbol{B}$ is the vector cross product of the ion velocity and the magnetic field, m is the mass of the ion, $\boldsymbol{E}$ is the electric field strenght and $\boldsymbol{a}$ is the acceleration. The equality of the forces leads to a differential equation for motion for charged particles:

$$(m/Q)\boldsymbol{a} = \boldsymbol{E} + \boldsymbol{v} \times \boldsymbol{B}, \tag{2.4a}$$

where

$$\boldsymbol{a} = \frac{d^2x}{dt^2} \tag{2.4b}$$

Since z=Q/e is the number of elementary charges, the equation explains how the ions are separated in the analyzer according to their different m/z values.

Different kinds of instruments can be used for this purpose. These are for example (i) a sector field mass analyzer, which uses an electric and magnetic field to affect the path and/or velocity of the charged particles, (ii) time-of-flight analyzer, which uses an electric field to accelerate the ions through the potential and then determines the time they need to reach the detector, (iii) a fourier transform ion cyclotron resonance analyzer, (iv) an orbitrap, etc. In present thesis a mass spectrometer with an quadrupole analyzer has been used and will be explained in more detail.

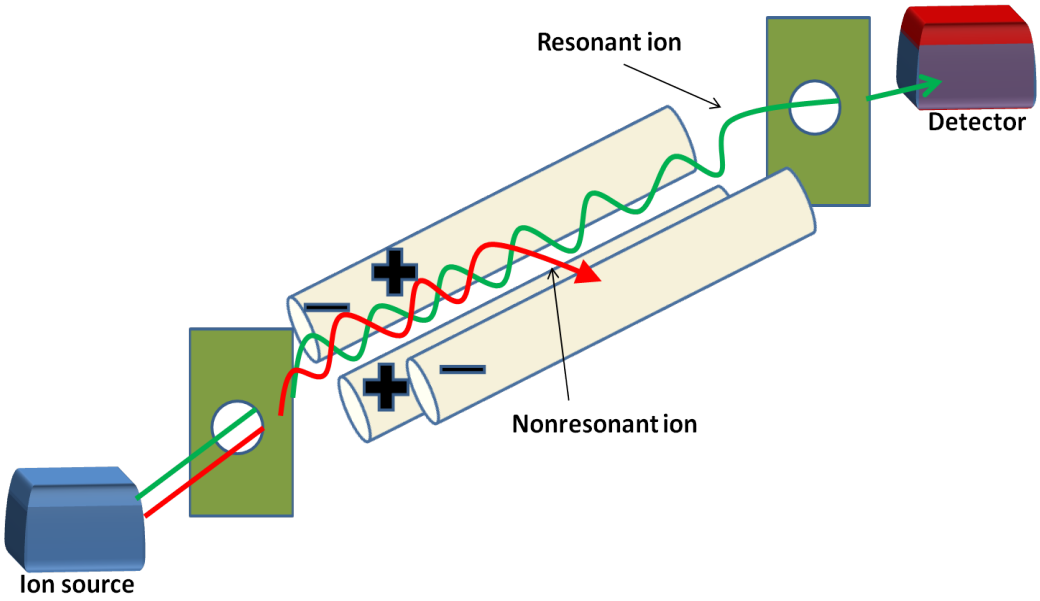

Fig. 2.6: Schematic compositon of QMS.

As is seen in the Fig. 2.6, the ions generated in the ion source pass through ion optical system, which accelerates and focuses the ions through an aperture into the quadruple filter. After passing the filter the ions pass again through an exit aperture before reaching the detector. The quadrupole analyzer itself consists of four metal rods arranged in a par-

allel way with the precisely same spacing between each other in the corners of a square. Two opposite rods have a potential of (U+Vcos(ωt)) and the other two rods have a potential of -(U+Vcos(ωt)) applied, where U is a constant voltage component and Vcos(ωt) is a sinusoidal voltage component. The applied voltage affects the trajectory of the ions traveling through the analyzer. For a given pair of U and V voltages only ions with a certain mass-to-charge ratio can pass in between the four rods and reach the detector. The other ions are thrown out or collide with the rods. By tuning the voltages U and V it can be scanned through a large spectrum of the m/z values. There are two methods for the voltage variation: either ω can be varied and U and V held constant or U and V can be varied for a constant ω.

In the last step the separated ions have to be detected. An electron multiplier, Faraday cup or ion-to-photon detector can be applied. Different detectors according to their sensitivity were used in present experiments. In the pressure range 10^{-3} - 10^{-5} mbar the ions can be more easily identified, as the higher number of ions produces a higher signal, which can be detected by the means of a Faraday cup. This detector consists of a conductive metal cup, which catches the incoming ions. The number of ions impinging in a given period is directly proportional to the electron current needed for neutralization. There are two shortcomings in the use of a Faraday cup: (i)the emission of low-energy secondary electrons from the surface and (ii) backscattering of the incident particles. Especially in the case of electrons, it is impossible to distinguish between incident electrons and backscattered electrons or fast secondary electrons.

For lower gas pressures leading to lower ion currents a secondary electron multiplier (channeltron) is employed. A channeltron can amplify the weak signal in an electron multiplier. In a process called secondary emission, a single electron can, when bombarded on secondary emissive material, induce emission of roughly 1 to 3 electrons. A channeltron is constructed as a funnel of glass coated inside with a thin film of semi-conducting material, with negative high voltage applied at the wider input end, and positive voltage near ground applied at the narrower output end (Fig. 2.7). Electrons emitted at any point are accelerated down the funnel before impacting the surface on the opposite side of the funnel. This process is repeated many times and results in an avalanche of electrons. At the destination end a separate electrode collects the multiplied electrons. The limit of this detection method is given by its high amplification: it cannot be operated at high gas pressures without risking damage due to high electron current.

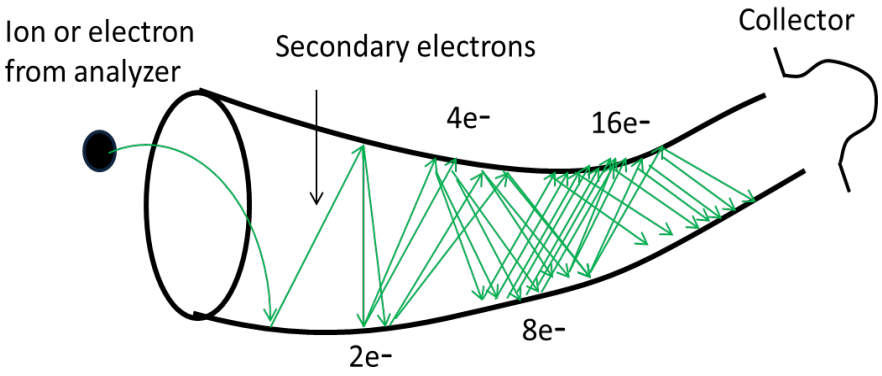

Fig. 2.7: Illustration of an electron multiplying effect of the channeltron.

2.4 X-ray photoelectron spectroscopy

The technique used to obtain chemical information from the surface of the sample is the X-ray photoelectron spectroscopy (XPS), also often called ESCA (electron spectroscopy for chemical analysis) [26]. The analyzed surface is irradiated by X-ray photons which have enough energy to excite core level electrons. Typically Al K_α radiation with the energy of 1486.6 eV or Mg K_α radiation with the energy of 1253.6 eV are used [27].

During the irradiation of the sample with an X-ray photon an ejected photoelectron leaves behind a core hole which can be filled by an electron from a higher energy level. The energy won from this transition can either be released as characteristic X-ray photon or be given up to another electron in the same or higher shell. The result of the later

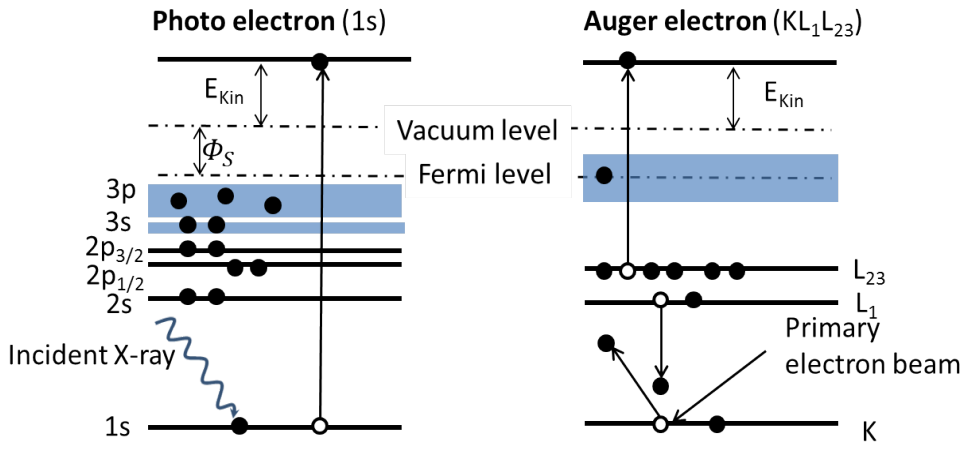

Fig. 2.8: Schematic energy level diagramm for the photoelectric and Auger process.

process is a second ejected electron, named Auger electron [28]. The Auger electrons, as schematically shown in the Fig. 2.8 are noted by the name of the shell from which the electron has originally been emitted, the shell from which the electron came to fill in the hole and the shell of the electron to which the energy has been transferred respectfully. Photoelectron peaks are noted by the name of the orbital from which the emitted electron came from.

The emitted photoelectrons can be analysed by an energy analyzer and form a spectrum: number of photoelectrons as a function of their kinetic energy. From the kinetic energy, the corresponding binding energy can be determined using the Einstein's equation (2.1). In the photoelectron spectrum (Fig. 2.9) the Auger peaks can easily be distinguished from the XPS peaks, since Auger peaks have kinetic energies which are independent of the ionizing radiation.

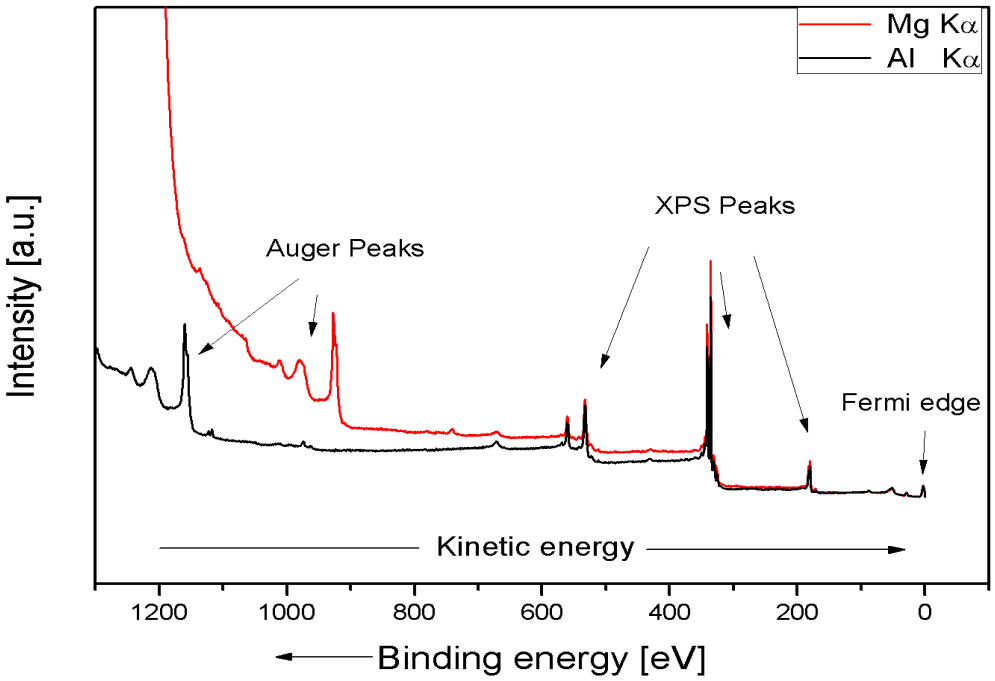

Fig. 2.9: Wide scan XPS spectrum of PdZr_3 (0001) taken with an Al- and Mg- anode.

Photoelectron peaks from orbitals with higher principle quantum number than 1 exhibit a spin-orbit splitting. Instead of one peak a closely spaced doublet occurs in the spectrum. This is due to a coupling between the unpaired spin and orbital angular momenta. Spin-orbit coupling can be treated with the Russell-Saunders coupling approximation. According to the approximation the final ionised state of Pd, the $(3d)^9$ configuration gives rise to two states which differ slightly in energy and their degeneracy g_J:

$$\mathbf{2}d_{\mathbf{5/2}} : g_J = 2 \times \{5/2\} + 1 = 6$$

$$\mathbf{2}d_{\mathbf{3/2}} : g_J = 2 \times \{3/2\} + 1 = 4$$

The relative intensity of the two peaks reflects the degeneracies of the final states ($g_J = 2J+1$), which in turn determines the probability of transition to such a state during photoionization. J is the total angular momentum. The resulting Pd $3d_{5/2}$ and $3d_{3/2}$ peaks will thus appear in the XPS spectrum with the ratio of the peak area 3:2.

The chemical shift and asymmetry of the peak gives information about the chemical state of the element and its physical surroundings. Atoms of higher positive oxidation state exhibit a higher binding energy due to the extra coulombic interaction between the photo-emitted electron and the ion core.

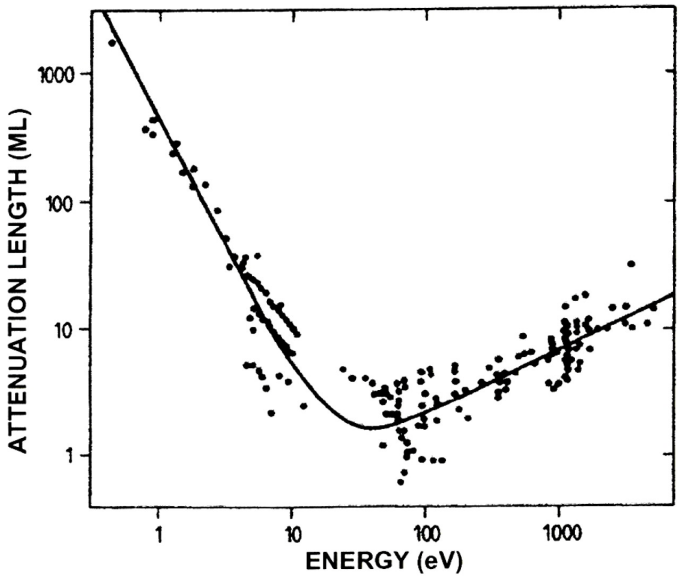

Fig. 2.10: Compilation of measurements of IMFP as function of electron kinetic energy; the solid line is the "universal curve" representing an "average" variation of the IMFP with the initial electron energy.

The reason why photoelectron spectroscopic techniques are surface sensitive can be explained by the dependence of the inelastic mean free path (IMFP) on the energy of electrons. Seah and Dench [29] compiled many of published UPS measurements on different solids for energies in the range 0 - 10 000 eV above the Fermi level, and established the so called "universal curve" for the variation of the IMFP with the initial electron energy (Fig. 2.10).

In XPS the typical secondary electron kinetic energies are between 250-1500 eV. From the curve in the Fig. 2.10, it can be said, that these electrons originate from the depth of about four to eight monolayers. In the Fig. 2.11, the surface sensitivity is illustrated by the exponential decrease of the intensity from deeper layers: ca. 70% of the signal emanates from a depth of less than λ and ca. 20% originates from the outermost layer.

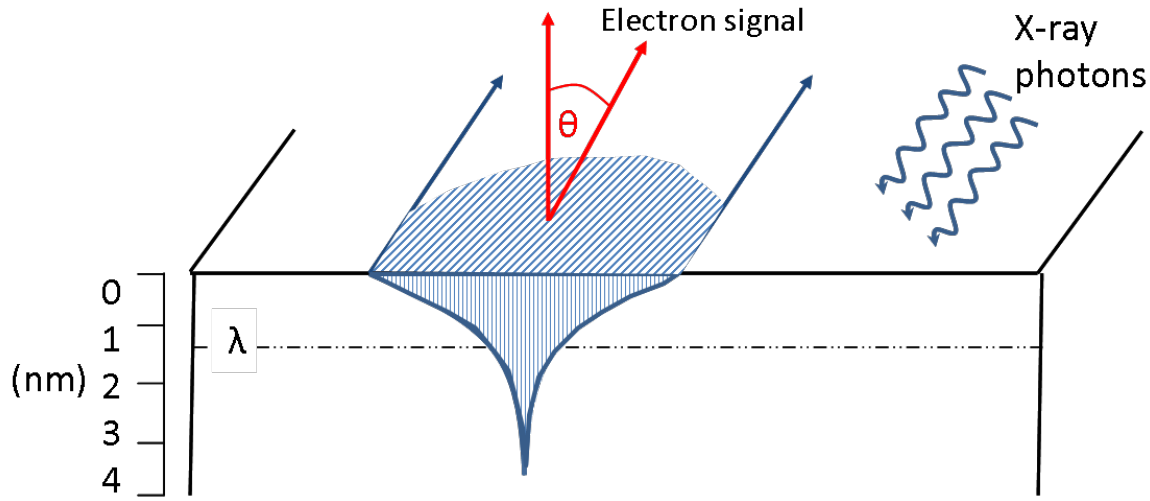

Fig. 2.11: The depth analysis in electron spectroscopy.

In the XPS spectrum it is important to be able to distinguish the photoelectron lines from the disruptive signals and get the right information from the spectrum. The true photoelectron lines are the most intense, narrowest and relatively symmetrical. The photoelectron lines of metals however, can exhibit asymmetry due to coupling with conduction electrons. Auger lines are group of lines in rather complex patterns. The four main series of Auger lines observable in XPS spectra are KLL, LMN, MNN and NOO series (Fig. 2.9).

Another effect which can be seen in the spectrum are X-ray satellites. These are due to the use of a nonmonochromatic source which exhibits next to the characteristic X-ray radiation also some minor components at higher photon energies. This results in a family of minor peaks at lower binding energies next to a normal photoelectron peak. Their intensity and spacing depends on the anode material of the source. Occasionally so called X-ray ghost lines can be observed in a spectrum. These are caused by impurities in the anode materials, as for example Mg impurity in Al anode or *vice versa*, Cu from the anode base structure or oxidation of the anode. X-radiation originating from these impurities to the sample, causes small peaks corresponding to the most intense spectral peaks but

displaced by a characteristic energy interval. Other disruptive lines in a spectrum are the shake-up lines. There is a finite probability that the ion after radiation will be left in an excited state. The kinetic energy of the emitted photoelectron in this case is reduced by the difference between this excited state and the ground state. The result is a satellite peak a few electron volts higher in binding energy than the main peak.

Interpretation of the XPS spectrum starts by identification of the lines. For simply identifying the elements which are in the sample a so called wide scan can be used. The characteristic binding energies for each element can be taken from well-established databases. In this work mainly the NIST X-ray Photoelectron Spectroscopy database (http://srdata.nist.gov/xps/) has been used. For detailed analysis a narrow scan of the main peaks should be recorded.

The element identification results simply from the fact, that no two elements exhibit the same binding energies of their core level electrons. Also change in the chemical environment can be followed by a change in the kinetic energy of the emitted photoelectrons.

XPS spectrum can also be used for quantification of the surface composition. The number of photoelectrons per second in a specific spectra peak is given by the equation 2.4 [27]:

$$I = nf\sigma\theta\gamma\lambda AT \tag{2.4}$$

where n is the number of atoms of the element per cm^3 of the sample, f is X-ray flux in photons/cm^2sec, σ is the photoelectric cross-section for the atomic orbital of interest in cm^2, θ is an angular efficiency factor for the instrumental arrangement based on the angle between the photon path and detected electron, γ is the efficiency in the photoelectric process for formation of photoelectrons of the normal photoelectron energy, λ is the mean free path of the photoelectrons, A is the area of the sample from the photoelectrons are detected and T is the detection efficiency for electrons emitted from the sample. The term $f\sigma\theta\gamma\lambda AT$ can be defined as the atomic sensitivity factor S. From the equation 2.4 the C_x (atomic fraction of the element x) can be obtained by:

$$C_x = \frac{n_x}{\sum n_i} = \frac{I_x/S_x}{\sum I_i/S_i} \tag{2.5}$$

For the value of I, the area of the peak in XPS spectrum can be used and the sensitivity factor S is an empirical factor taken from literature [30].

The instruments needed for a XPS measurement are X-ray source, UHV chamber with a pumping system, electron energy analyzer and detector. The photoelectrons emitted

from the sample first pass through a lens system, which has the purpose to focus the electron flux from the sample surface to the entrance slit of the analyzer. The most used electron-energy analyzer for XPS is the concentric hemispherical analyzer, where two hemispheres are positioned concentrically. The photoelectrons are first retarded to a constant pass energy in the range between 20 and 100 eV before reaching the entrance slit. Negative potentials are applied to both the inner and outer hemisphere, so that only electrons with certain kinetic energies will arrive at the detector side of the analyzer. By changing the potentials selectively electrons of particular kinetic energies can pass through the analyzer. As a detector several single channeltrons or a channel plate can be used.

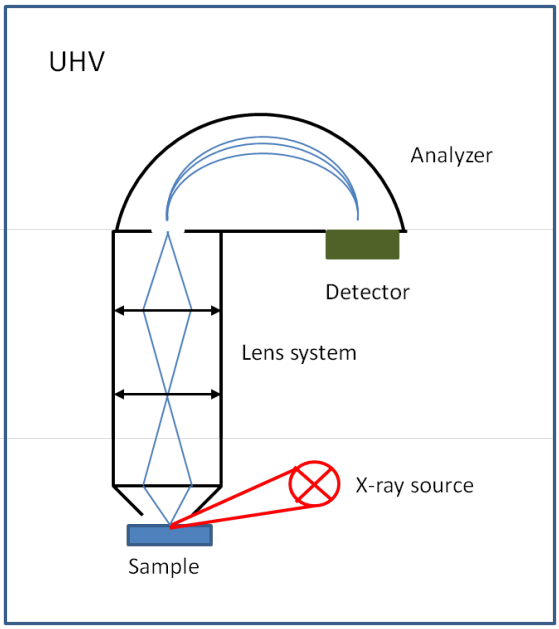

Fig. 2.12: Schematic composition of an XPS setup.

The experimental XPS setup used in present work was a SPECS instrument containing the XR 50 X-ray source with a twin anode (Al, Mg) and a cooling unit and Phoibos 100 energy analyzer.

The complete X-ray source consits of the X-ray source module XR 50, the power supply XRC 1000 and the cooling unit CCX 60. The source is installed on a z-shift manipulator, allowing the X-ray source to move from the XPS position to a parking position further away from the sample, if other operations, such as transfer, Ar^+ bombardment of the sample or sample annealing are beeing carried out. The irradiated area on the sample is elliptically shaped, with area of 1 - 2 cm^2 depending on anode-sample distance. The Phoibos 100 hemispherical electrostatic energy analyzer allows recording of energy spectra for nega-

tive and positive particles in the kinetic energy range from 0 eV to 3.5 keV with minumum steps of 7 meV. It has a multi-element, two stage transfer lens, which can be operated in several different modes for angular and spatially resolved studies. A Slit-Orbit mechanism and a Multi-Mode Lens make the sampling area of the analyzer and the acceptance angle area of the lens selectable, thus allowing the analyzer to spatially resolved measurements down to a diameter of 100 μm as well as large area investigations associated with different lens acceptance angles. The analyzer is equipped with a channelplate and aditionally a 2D CCD detector consisting of a 40 mm diameter Micro-channel plate with a phosphor screen, which can be also used for imaging of the sample via XPS.

The software used for operating all units during XPS measurements was SpecsLab2 and the software for spectrum evaluation was CasaXPS. The sample in the "XPS chamber" is set on a movable manipulator allowing positioning in x-, y- and z- direction, but also tilting of the sample for angle resolved measurements.

CHAPTER 3

CO OXIDATION ON PALLADIUM FOIL

In this chapter results of CO oxidation experiments performed on palladium micrograins of the Pd foil sample, and experiments on the foil after oxidizing treatment are presented.

Formation of oxides on metal surfaces has recently won much attention of catalysis research groups, driven by the discovery, that some metal oxides are the active phase in catalytic reactions, e.g. RuO_2 has been found active for the catalytic CO oxidation, following the Mars-Krevelen mechanism [31].

Oxides of noble metals are usually formed only at high partial oxygen pressures and elevated temperatures and thus can hardly be observed in UHV studies. However other oxides of less catalytically active elements can be formed, e.g. the observation of bulk dissolved silicon as the cause of oxide formation on Pt(111) surfaces has first been mentioned by Niehus and Comsa [32], followed by the study of this effect by Bader [33] on palladium. Until now this effect has been neglected in studies of the catalytic CO oxidation reaction on platinum group metal surfaces.

In present thesis the formation of silicon oxide from bulk silicon, present as an impurity in used palladium samples and its effect on the activity of the Pd surfaces towards the CO oxidation reaction are studied.

3.1 Pd foil sample

The sample investigated in this chapter has been a polycrystalline palladium foil (AlfaAesar, 99.9% purity) which is composed of 50-100 μm large grains of different crystallographic orientations formed after heating the sample for several hours at 1100 K in UHV. The sample is attached to a stainless steel sample holder, which can be locked with the

transfer rod, so that the sample can be moved from the "PEEM chamber" to the "XPS chamber".

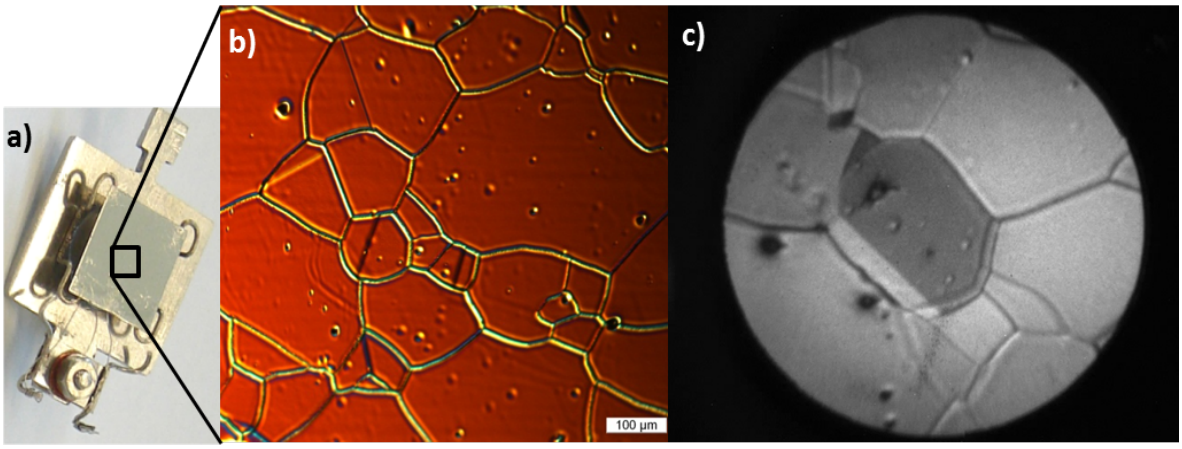

Fig. 3.1: a) 10×10 mm Pd foil sample on the sample holder. b) Microscopic image of the same sample. c) PEEM image of the same sample.

3.2 Sample preparation

In order to obtain an atomically clean surface, the Pd foil has been Ar^+-sputtered (argon pressure: 6-8×10^{-6} mbar, ion current of ≈ 3μA and kinetic energy of 1 keV) for 15 minutes and consequently annealed at 800°C for another 15 minutes. An unavoidable and disturbing contamination present on the surface is carbon, which was eliminated by heating the sample in oxygen atmosphere (5×10^{-7} mbar) for 15 minutes during which the surface carbon was removed by the reaction with oxygen. This procedure was performed prior to each experiment.

3.3 Experimental results for the CO oxidation on the Pd foil

3.3.1 Annealed Pd foil

The CO oxidation on the palladium foil was followed by MS and PEEM to obtain both global and local reaction kinetics. During the measurements the oxygen partial pressure has been held constant at 1.3×10^{-5} mbar and monitored by both MS and a spinning rotor gauge and the temperature has been held constant at 160°C. The CO partial pressure, has been increased, until the transition from an oxygen- to a CO-covered surface (τ_A) has

been observed and thereafter decreased until the reversed transition, τ_B occurred. In the Fig. 3.2 the CO_2 rate during such CO pressure cycle obtained by MS as a function of CO partial pressure is shown and the hysteresis behaviour of the CO oxidation on Pd foil is documented. Both kinetic transtitions, τ_A and τ_B, could be determined from the sudden decrease and increase of the reaction rate in Fig. 3.2.

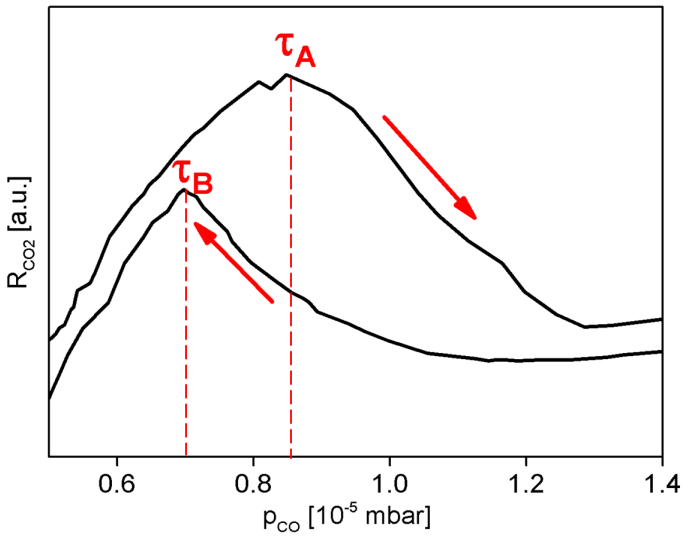

Fig. 3.2: CO_2 reaction rate determined by MS as a function of CO pressure during the CO oxidation reaction (p_{O_2}= 1.3×10^{-5} mbar, T= 160 °C). The direction of the increasing and decreasing CO pressure during the CO pressure cycle is indicated by red arrows.

PEEM has been used to image *in situ* the reaction on the annealed Pd foil surface. A clean palladium surface is a very suitable sample for following the kinetic transitions in PEEM, since the reaction fronts are clearly visible. As the poisoning of the surface by CO coverage begins, dark fronts formed at different times for different (hkl) planes can be observed in PEEM. The observation, that the Pd(111) domain is the first one which becomes poisoned is in agreement with the well known fact, that this plane is the most densely packed. The reaction fronts which appear during the hysteresis experiments on an annealed surface are portrayed in the Fig. 3.3.

Since the individual grains behave independently in the CO poisoning, the brightness of the grains with different crystallographic orientations in the PEEM video can be quantified and used for local kinetic measurements. This has been done for three chosen grains with low Miller indices, namely Pd(111), Pd(110) and Pd(100), which have previously been identified with the EBSD (electron backscattering diffraction) method. The plot of the local PEEM intensity for individual grains as a function of CO partial pressure shows, sim-

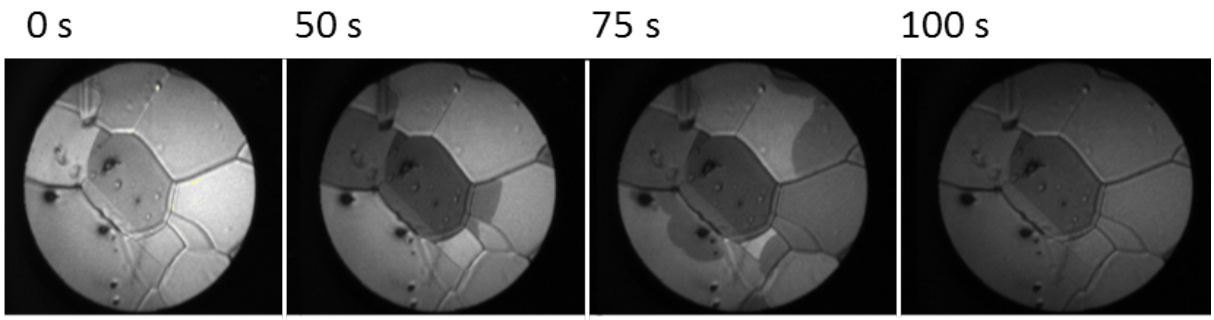

Fig. 3.3: PEEM video frames of the CO oxidation reaction on the annealed Pd foil during the τ_A kinetic transition (p_{O_2}= 1.3×10^{-5} mbar, T= 160 °C). The bright parts of the foil are oxygen-covered, the dark parts are CO-covered.

ilary as for the case of MS curve, a hysteresis with a pronounced bistability region (Fig. 3.4).

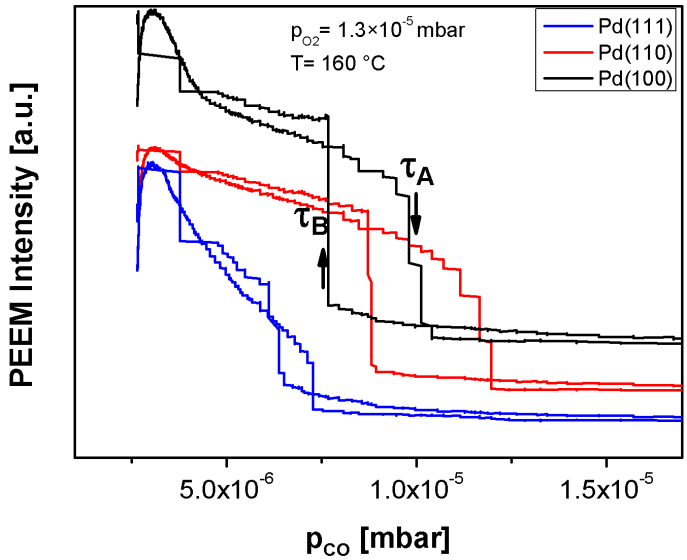

Fig. 3.4: Local reaction kinetics: PEEM Intensity as a function of CO pressure for (111), (110) and (100) planes of the annealed palladium foil during CO oxidation reaction hysteresis experiment.

In Fig. 3.4 the kinetic transition points τ_A and τ_B are visible: the transition to a CO-covered surface, τ_A, is detectable in PEEM by the sudden decrease in the intensity, the second transition to the oxygen-covered surface, τ_B, is seen in the sudden increase in the intensity. As already mentioned, the first domain to become CO poisoned is the Pd(111) domain, followed by Pd(100) and Pd(110) is poisoned last.

3.3.2 Pd foil after oxidizing treatment

3.3.2.1 Oxidizing treatment

The Pd foil has been treated at higher oxygen pressures (5×10^{-6} mbar) and elevated temperatures for 15 minutes. In order to follow the influence of the temperature on the oxidizing process, the treatment has been carried out at temperatures from 400°C to 600°C with 100°C steps and from 600°C to 700°C with 50°C steps.

3.3.2.2 Kinetic measurements

For the oxidized Pd foil the kinetic reaction measurements with MS and PEEM during the CO pressure cycle under same isothermal conditions as for the annealed foil were performed. It has been observed, that already relatively low oxidizing temperatures (400°C) cause a decrease in the CO_2 reaction rate. This effect becomes more significant for higher oxidizing temperatures (Fig. 3.5).

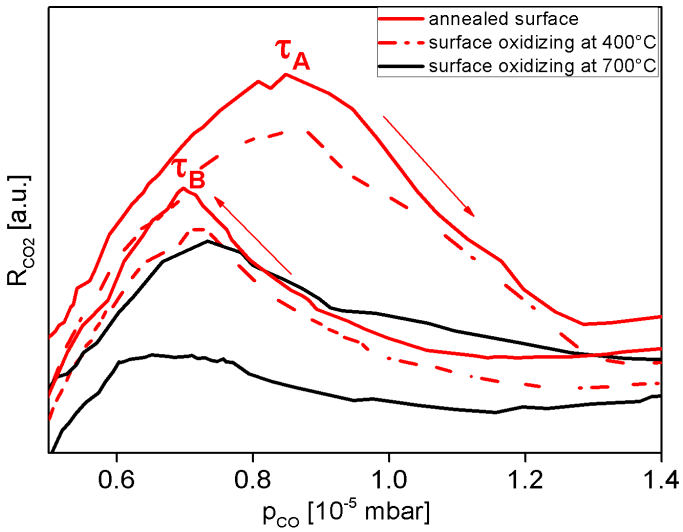

Fig. 3.5: CO_2 reaction rate determined by MS as function of CO pressure during the CO oxidation reaction hysteresis experiment on the annealed and oxidized Pd foil. Three curves are shown: red for reaction on clean Pd surface, dashed red for the reaction on the surface after oxidizing treatment at 400°C, black for the reaction on the surface after oxidizing treatment at 700°C. The direction of the CO pressure cycle is indicated by red arrows for the curve of the annealed Pd surface.

Imaging of the Pd foil surface during CO oxidation with PEEM, that has previously been treated with oxygen shows a dramatically different result than imaging of the annealed Pd surface. The palladium foil surface appears much darker in PEEM after the oxidizing

treatment (Fig. 3.6), due to a significant increase of the surface work function. During the reaction no fronts were observed, the surface becomes gradually darker or brighter, without a differentiating between individual grains. The direct comparison of the change in PEEM intensity during CO oxidation hysteresis experiment for the annealed and oxidized surface is shown in Fig. 3.7.

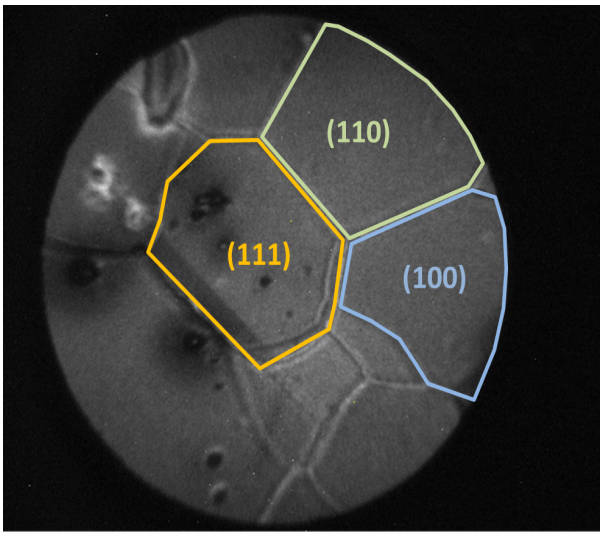

Fig. 3.6: PEEM image taken during the CO oxidation hysteresis experiment on a palladium surface after oxidizing treatment at 700 °C and 5×10^{-6} mbar oxygen pressure.

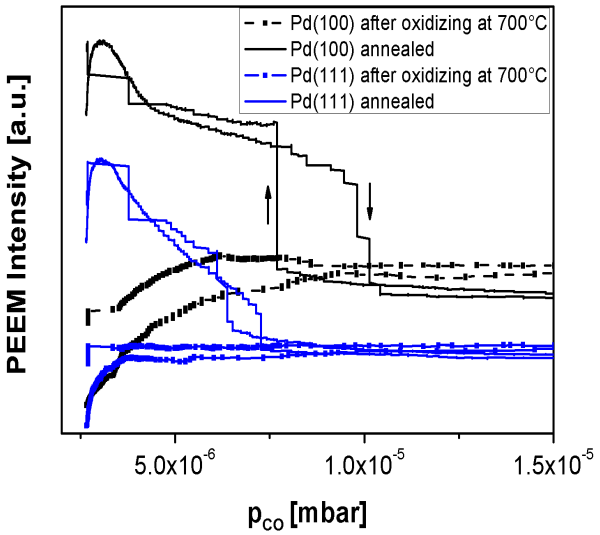

Fig. 3.7: Comparison of the local kinetics for a Pd(111) and Pd(100) domain before and after the oxidizing treatment at 700 °C and 5×10^{-6} mbar oxygen pressure.

To follow the changes of the work function with increasing oxidizing temperature a PEEM image after the oxidation has been recorded and its intensity has been quantified. The intensity of a PEEM image varies by a certain amount depending on the exact position of the sample in front PEEM, pressure and temperature. Because of this variation a reference intensity of a clean surface before oxidizing has been taken before each oxidizing treatment. Finally the quotient of the PEEM intensity of the image after and before oxidizing was compared.

The experiment has been carried out as follows. After the cleaning process of the sample a PEEM image with reference intensity for a certain position of the sample and certain parameters has been obtained. All images were taken at the same temperature of 200 °C and same oxygen pressure of 5×10^{-6} mbar. Thereafter the temperature was increased until the aimed oxidizing temperature and held for 15 minutes. The image of the oxidized surface was taken at the same conditions as the reference image recorded after cooling

back to 200 °C, keeping the position of the sample in front of PEEM the same and oxygen pressure constant.

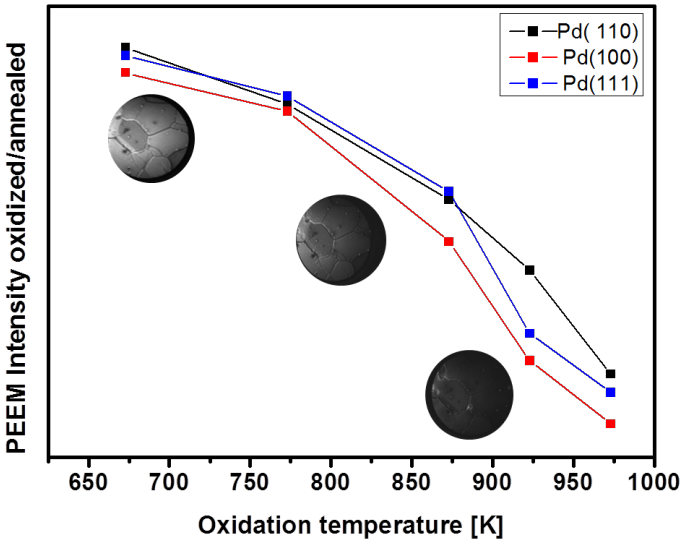

Fig. 3.8: Normalized intensity of the PEEM image: $I_{oxidized}/I_{reference}$ as a function of oxidizing temperature for Pd(111), Pd(100) and Pd(110) domain.

As a result, a pronounced decrease of the normalized intensity and thus the increase of the work function of all observed (hkl) planes for increasing oxidizing temperatures has been obtained (Fig. 3.8).

3.3.2.3 Results of XPS measurements

To explain the deactivation of the surface after the oxidizing treatment, which has been observed globally for the whole foil with MS as well as locally for individual (hkl) planes with PEEM, chemical information about the surface was obtained. Directly after performing the kinetic measurements, the sample has been transferred to the "XPS chamber" and analyzed. A survey spectrum of the sample showed mainly the peaks of palladium, oxygen, carbon and silicon. The focus of the measurements has been directed towards the Pd 3d doublet and the Si 2p peak, which have been measured in a narrow scan 5 times to obtain a smooth signal line.

The palladium 3d peak has shown no change after the oxidizing treatment (Fig. 3.9), which means that at present oxidizing conditions no Pd surface oxide is formed. Some groups have observed the formation of surface oxide Pd_5O_4 after oxidizing treatment at 400 °C and 5×10^{-6} mbar oxygen pressure [34], however in our system, this has not been

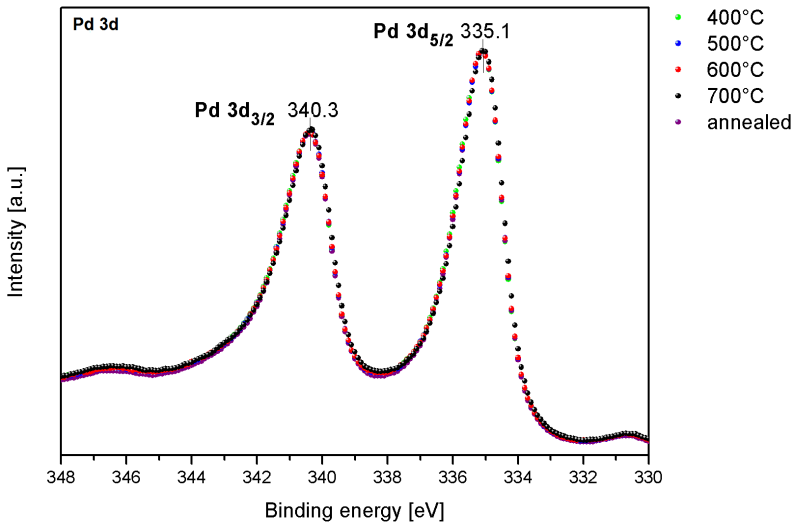

Fig. 3.9: XPS Pd3d region of the Pd foil: total overlap of 3d spectra of the metallic Pd foil and the same foil after oxidizing treatment at 400 °C, 500 °C, 600 °C and 700 °C and 5×10^{-6} mbar oxygen pressure. The peak maximum of $3d_{3/2}$ peak is at 340.3 eV and $3d_{5/2}$ at 335.1 eV, corresponding to metallic Pd [27].

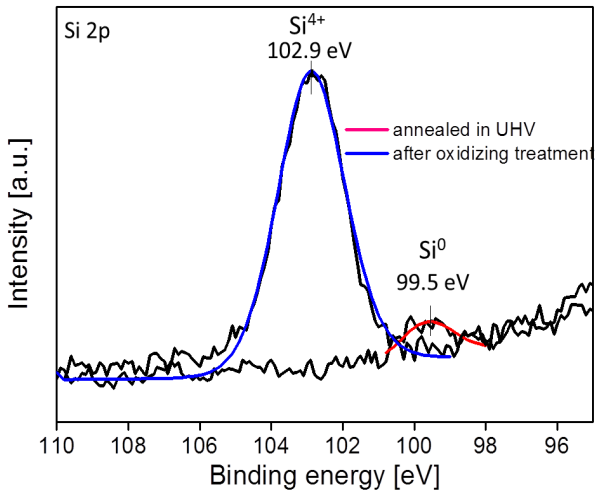

Fig. 3.10: XPS Si 2p region of the Pd foil: comparison of the spectra for the annealed Pd foil surface (red) and the same surface after oxidizing treatment at 700 °C and 5×10^{-6} mbar (blue).

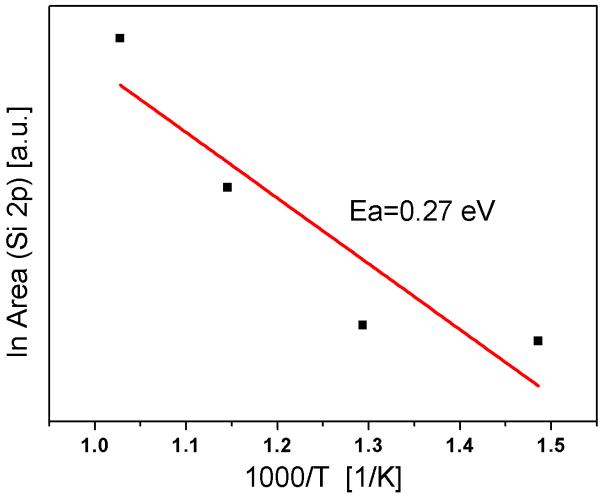

Fig. 3.11: Arrhenius plot for the effective activation energy of the Si segregation from the bulk of palladium to the subsurface area and consequent oxide formation.

achieved, even after oxidizing treatment at higher oxygen partial pressures (up to 10^{-4} mbar oxygen pressure). The proof for the absence of palladium oxides is shown by the overlap of the narrow scans of the Pd 3d XPS peaks before and after oxidizing treatment of the Pd foil at different temperatures (Fig.3.9). From these XPS data we can conclude,

that the observed change in activity after oxidizing treatment, has not been influenced by the change in chemical state of palladium.

In contrary to Pd 3d peaks, the narrow scan of Si 2p peak has shown a significant change after the oxidizing treatment. The Si 2p peak area has grown during the oxidizing treatment and has shifted to higher binding energies. This can be explained by the increase in the concentration of silicon on the surface and also by change of its chemical state. As is seen in the Fig. 3.10 the Si 2p peak after the oxidizing treatment is shifted by 3.4 eV to higher binding energies, which is typical for SiO_2 formation (NIST XPS database). With increasing oxidizing temperature, the concentration of silicon oxide on the surface has grown as observed by the increase in the area of the XPS Si 2p peak. The Si 2p peak areas have been used to determine the effective activation energy of the segregation process and the oxide formation from the slope of the Arrhenius plot.

The determined effective activation energy of 0.27 eV is remarkably low compared to a known activation energy for thermal oxidation of silicon, which is around 2 eV [35, 36] . The known Deal-Grove model of thermal SiO_2 formation [35] is based on the assumption that Si oxidation proceeds by the transport of molecular oxygen from the ambient to the Si/SiO2 interface through already oxidized Si layers and does not apply here. In our case, the rate of SiO_2 formation is not limited by the oxygen diffusion, but by the silicon transport from the Pd subsurface region to the surface. The process of SiO_2 formation studied in the present work can be illustrated by Fig. 3.12. Molecular oxygen adsorbs dissociative to the palladium surface, and thus atomic oxygen takes part in the oxide formation. It is clear that, the activation energy values typical for the oxygen diffusion limited process could not be expected in present case.

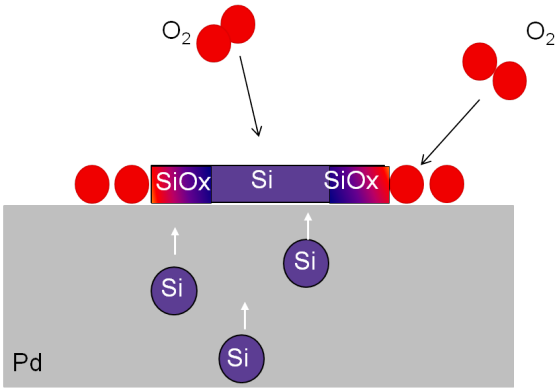

Fig. 3.12: Illustration of the Si segregation from bulk palladium and consequent silicon oxidation by atomic oxygen adsorbed on palladium surface.

Recently, unusually small activation energy values of e.g. 0.13 eV [36] or even lower [37] were observed for the oxidation procedure where the oxygen diffusion limit was lifted by using atomic oxygen for the Si oxidation. Generally, experimental observations are known, which show that the presence of oxygen (even in the 10^{-6} mbar range) increases the mobility of Si in Pt-metals causing the precipitation of SiOx at the surface [38]. However in the present study first systematic studies of this effect have been performed and effective activation energy has been determined. The enhanced Si segregation in the presence of oxygen can be rationalized considering energetic arguments: the higher bonding strength of Si on an oxygen-covered Pd surface provides an energetic sink for Si atoms due to the chemical potential gradient, facilitating thus the Si segregation and following SiO_2 formation.

The segregation of Si to the surface of the Pd-Si alloy is actually the first step of an effect known for multicomponent systems as surface-directed spinodal decomposition [39, 40]. A rapid change of system parameters (e.g. temperature, pressure) can lead to a phase separation of phases of a multicomponent system. In the presence of a surface, this process may be influenced by the wetting tendency of the surface by one of the phases and if one of the components is preferentially attracted or repelled from the surface. This results in the formation of anisotropic surface-directed concentration waves which form a layered periodical structure parallel to the surface. This effect has been observed for liquids and polymer films, but can occur also in metallic alloys on a macroscopic scale [41].

In our case the Si-phase is drawn to the surface due to the presence of oxygen and elevated temperatures enhance the diffusion process. Since there is no thermodynamic barrier to the reaction inside of the spinodal region, the decomposition is determined solely by diffusion and therefore can be treated purely as a diffusional problem. The modulation by spinodal decomposition in an initially homogeneous system implies an uphill diffusion, however the negative diffusion coefficient would not explain the formation of periodical structures during this process, which was observed for some alloy systems. The first explanation of the periodicity was given by Hillert, who solved the flux equation numerically and found that inside the spinodal region it yielded a periodic variation of composition with distance [42]. An even better model for this process has been developed by Cahn, who included the effects of coherency strains as well as the gradient energy term [43].

3.4 Summary

CO oxidation on Pd foil has been studied by the PEEM and MS techniques. The hysteresis behavior of the reaction has been observed during a CO pressure cycle experiment under isothermal conditions and the global kinetic transitions from an active to an inactive surface were determined by MS. The intensity of the PEEM video has been quantified and the local kinetic transitions for low index orientations have been determined.

Silicon is a common impurity present in commercial Pt group catalysts. The segregation of this element from subsurface area to the surface of the catalyst, a palladium foil, has been observed after oxidizing treatment at oxygen pressure of 5×10^{-6} mbar and temperatures between 400 °C to 700 °C by the increase of the XPS Si 2p peak. The formation of SiO_2 was concluded from the observed Si 2p peak shift of 3.4 eV to higher binding energies. The effective energy for this process was determined from the Arrhenius plot of the Si 2p XPS peak area and was found to be 0.27 eV. The SiO_2 formation on the surface of palladium foil led to deactivation of the catalyst in respect to the CO oxidation reaction, which was shown by the results of the kinetic measurements by MS and PEEM.

Present studies have shown, how already a small amount of impurities can lead to drastic change in the catalytic activity of palladium. The impurity, here special case of silicon, does not have to be detectable on the catalyst surface after cleaning procedure, but can diffuse to the surface from the bulk under reaction conditions. The presence of oxygen enhances the segregation of silicon from bulk and also forms a very stable oxide, which deactivates the surface for the CO oxidation reaction. Without surface analysis techniques, such as XPS applied *in situ*, one could interpret the effect as a palladium oxide formation and therefore come to the conclusion, that palladium oxide is the inactive phase for the CO oxidation. Therefore attention should be drawn to the contribution of impurities in catalysts, which can segregate to the surface under reaction conditions and might influence the catalytic activity. Especially the presence of oxygen, as observed in present work, may have profound effects on the surface concentration and solubility of impurity elements, such as Si.

CHAPTER 4

CO OXIDATION ON SUPPORTED PALLADIUM AND PALLADIUM OXIDE POWDER SAMPLES

In present chapter results of experiments performed on Pd and PdO powder samples are presented. It has been observed, how the morphology of the sample affects the catalytic CO oxidation reaction.

4.1 Pd powder in the CO oxidation

In real catalysis the reaction does not occur on the surface of a perfectly polished single crystal or foil with defined crystallographic orientations, but rather on oxide supported nanoparticles. Such configuration serves the purpose of dispersion of the catalyst and ensuring a large surface area for the reaction. In the previous chapter, experiments on palladium micrograins have been presented, here the comparison of this foil with a model consisting of palladium powder on alumina support will be discussed, in respect to the catalytic CO oxidation reaction. The presence of step edges, kinks, adatoms, vacancies, heteroatoms, impurities, grain boundaries and other defect sites on model particles strongly influence the surface properties, as has been observed for instance by scattering experiments, chemical reactions, crystal growth, epitaxy etc. [44].

Research done on single crystals has contributed to discoveries of some fundamental reaction mechanisms and after these were thoroughly studied, the attention of surface science has turned to investigating the influence of surface irregularities. Surface defects largely affect the sticking coefficient of gaseous molecules on surfaces, which explains the large scatter of values for sticking coefficients for the same system, but with different de-

fects [45]. The influence of step density on the oxygen adsorption and consequently the CO oxidation reaction has been studied by Hopster et al. [46] on a cylindrical Pt(111) surface, whose convex surface exhibits regions of different step densities. Their observation concluded, that oxygen adsorption increases linearly with increasing step density, independently of step orientation, however the oxygen adsorbed at these step sites is not available for the catalytic CO oxidation. The influence of steps has also been studied in an experiment, in which gold, silver or copper have been sputtered on the step edges of a Fe single crystal, in order to minimize the influence of these defects and follow the reaction on an almost perfect surface [47, 48]. From these and many more studies, it can be concluded, that defect sites are sites with differing activation barrier for adsorption [44].

Observing that the morphology of the investigated surface has a large influence on the catalytic activity raises the question, which chemical and physical properties of the surface irregularities may cause this influence. Most obvious of all, structural surface defects produce surface atoms, which are coordinatively unsaturated compared to regular surface atoms. Eigler and Schweizer [44] provided a very elegant proof of the higher adsorption energy for step and vacancy sites by "decorating" a Pt(111) surface with a small coverage of xenon atoms, after which most of the Xe atoms were found along the step edges. After "kicking away" one of the few Xe atoms, which have been held on a terrace with the STM tip, a vacancy site and thus the explanation for enhanced adsorption on the terrace has been found directly under this atom. The atoms near defects suffer a displacement from their regular 2D surface lattice sites. This unbalance leads to geometrical relaxation (in addition to the relaxation of the surface atom layer as whole), which in turn leads to a change of the local electronic structure.

In present thesis another contribution to studies of the influence of surface morphology has been made by comparing palladium powder on an alumina support, which is widely used in real catalysis, with a relatively smooth palladium foil in the activity towards the catalytic CO oxidation reaction.

4.1.1 The Pd powder sample

The sample studied in this part of the work has been a Palladium black in powder form (Fluka AG), which has been pressed into an aluminium foil using a pressing machine and a tantalum foil as a forcer. The powder was impregnated into the softer aluminium foil and a sample of 10×10 mm containing Pd powder has been fixed using a tantalum frame onto a stainless steel sample holder. This sample holder can be locked with the trans-

fer rod, so that the sample can be easily moved from the "PEEM chamber" to the "XPS chamber" and *vice versa*.

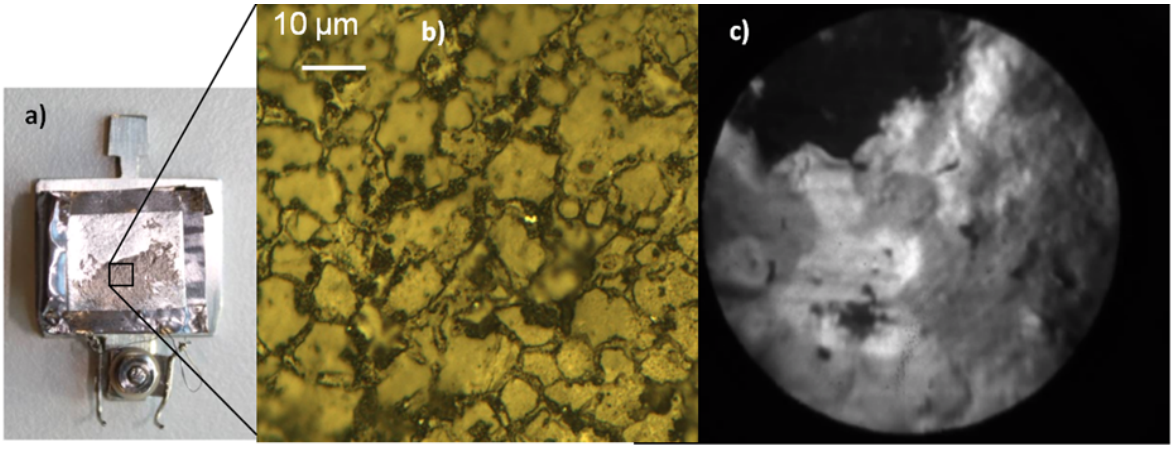

Fig. 4.1: a) The 10×10 mm "Pd powder on alumina" sample on the sample holder. b) Microscopic image of the same sample. c) PEEM image of the same sample during CO oxidation reaction.

4.1.2 Preparation of the Pd powder sample

Preparation of the supported Pd powder has been limited in heating by the low melting point of aluminium, which lies at 660°C . It has been observed, that already at temperatures lower than 400°C the aluminium foil has started to bend due to the thermal expansion and thus the PEEM imaging was hardly possible. Therefore the typical procedure consisted of 15 minutes of sputtering with Ar^+ ions (argon pressure: 6×10^{-6} to 8×10^{-6} mbar, ion current of $\approx 3\mu$A and kinetic energy of 1 keV), 15 minutes of heating at 350°C and 15 minutes of heating at the same temperatures, but in oxygen pressure of $\approx 5\times10^{-7}$ mbar to remove carbon impurities.

4.1.3 XPS control of the Pd powder sample

The chemical state of the sample after oxidizing treatment at different temperatures has been controlled by XPS. To identify all present elements a wide scan survey has been performed. Apart of the expected elements palladium, aluminium, tantalum and oxygen also small amounts of carbon have been detected. Tantalum is used to fix the sample to the sample holder and is therefore present in the spectrum.

The XPS measurements showed the $3d_{3/2}$ and $3d_{5/2}$ peaks at binding energies 340.4 eV and 335.1 eV, correspondingly (see Fig. 4.2). These values correspond to metallic palladium (NIST XPS database).

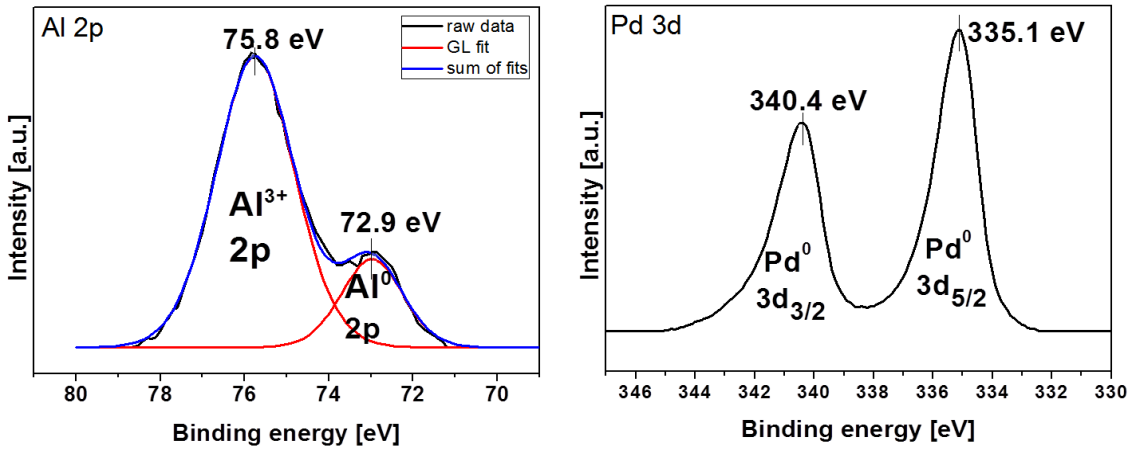

Fig. 4.2: Left: XPS spectrum of Al 2p region. The spectra show the large contribution of the oxidized aluminium and a small part of metallic Al in the signal. Right: XPS spectrum of Pd 3d region of the supported palladium powder sample. Pd is in its metallic state.

The XPS scan of the Al 2p region showed a peak with two maxima, 75.8 eV and 72.9 eV, which are assigned to the oxidized and metallic signal of aluminium, correspondingly. From the chemical shift of 2.9 eV to higher binding energies it can be concluded, that the surface of the support for the palladium powder consists mainly of alumina, Al_2O_3 (NIST XPS database).

4.1.4 Kinetic reaction measurements for the Pd powder sample

Kinetic reaction measurements during the CO oxidation reaction have been made for the supported palladium sample by MS and PEEM. Before any activity towards the catalytic CO oxidation could be observed, the sample had to be repeatedly treated by sputtering, heating and heating in oxygen as described in the Preparation section and exposed to the CO oxidation reaction conditions many times. The increase in activity observed by CO_2 rate in MS was accompanied by the decrease of the C 1s peak in XPS spectrum of the sample and also the appearance of reaction fronts in PEEM, which were not observable at the beginning.

During the PEEM imaging the absolute PEEM intensity of the Pd powder sample, has been significantly higher as any intensity so far observed by us for the palladium foil, which is in agreement with the fact, that a defect-rich surface has a lower work function [44].

As described in the first chapter, the CO oxidation on platinum group metals shows a hysteresis behavior under certain conditions. This effect has also been observed for the

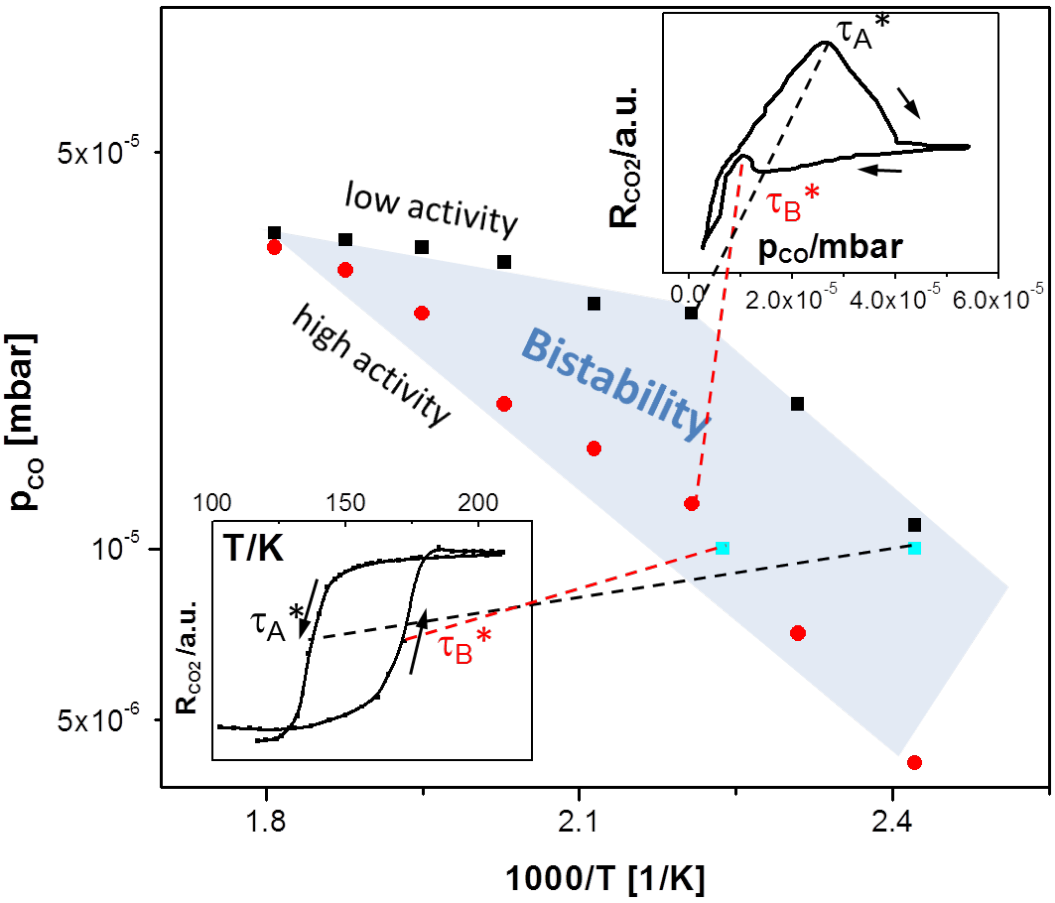

Fig. 4.3: Global kinetic phase diagram of the supported palladium black sample constructed from transition points as observed by MS with transition points (blue) from the "light-off" measurement (left down corner) The bistability region is indicated by blue colored area.

palladium powder sample and a kinetic phase diagram has been constructed. After the sample has been cleaned, the oxygen pressure of 1.3×10^{-5} mbar has been introduced to the chamber and the simultaneous measurement of MS and PEEM imaging has been performed. Keeping the temperature and partial oxygen pressure constant, the CO pressure has been increased until the PEEM image has been darkened and the reaction rate in MS has decreased, in other words until the kinetic transition from oxygen- to CO-covered surface (τ_A) has occurred. After that CO pressure was reduced and the CO pressure cycle was finished, after the second kinetic transition, τ_B i.e., from the CO-covered to the oxygen-covered surface has occured. The experiment has been repeated for different temperatures from 140 °C to 280 °C in 20 °C steps, always at the same oxygen partial pressure. In this way a global kinetic phase diagram has been constructed using the obtained kinetic transition points observed by MS (see Fig. 4.3). Simultaneously, the PEEM measurements

have been performed and a local kinetic phase diagram has been constructed from kinetic transitions detected by PEEM (see Fig. 4.4).

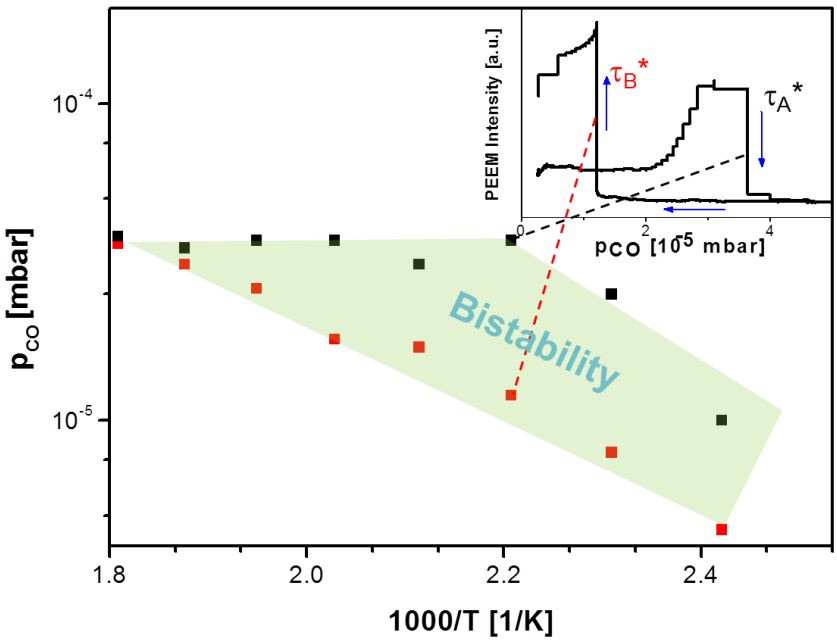

Fig. 4.4: Local kinetic phase diagram of the supported palladium black sample constructed from transition points as observed by PEEM. The bistability region is indicated by green colored area.

The measurements for the kinetic phase diagram have been performed under isothermal conditions. It is interesting to apply additionally a different approach for determining the kinetic transition points, namely a so called "light-off" experiment. The significance of such experiment lies in its parallel to the "cold-start" of the motor engine, during which most of the pollutants are emitted. Before the catalytic converter reaches its "ignition" temperature, it is inactive. A "light-off" experiment simulates the warming period and the increase in the activity can be observed exactly at the "ignition" temperature of Pd powder. For this experiment a constant oxygen pressure of 1.3×10^{-5} mbar and a constant CO pressure of 1.0×10^{-5} mbar were created inside the chamber. Under these conditions the surface of the Pd powder is covered with CO at 298 K. The temperature has been ramped, until a transition to the active state (τ_B) has been observed by both MS and PEEM and again decreased until the reversed transition (τ_A) occurred. The transition temperatures have been noted and the kinetic transition points of the "light-off" measurement have been compared with the already determined global kinetic phase diagram. As can be seen

in Fig. 4.3 the results of the isobaric "light-off" experiment is in agreement with previously obtained isothermal measurements.

The transition point to a CO-covered Pd surface, τ_A, characterized by a sudden decrease of the CO_2 rate in MS is also accompanied by a decrease in the PEEM intensity, since the CO-covered surface has a higher work function, than an oxygen-covered surface. The opposite is true for the reversed transition τ_B. In this way the transition points, τ_A and τ_B can be obtained from the integrated PEEM intensity over a defined area of the imaged surface. In contrary to the *in situ* PEEM imaging of the Pd foil with micrograins, the powder does not consist of regions, which are more resistant to the CO poisoning than others (different poisoning for Pd(111), Pd(110) and Pd(100) observed in chapter 3. The reaction fronts usually initiate in more points at the sample surface and spread outwards in all directions, forming a growing circle.

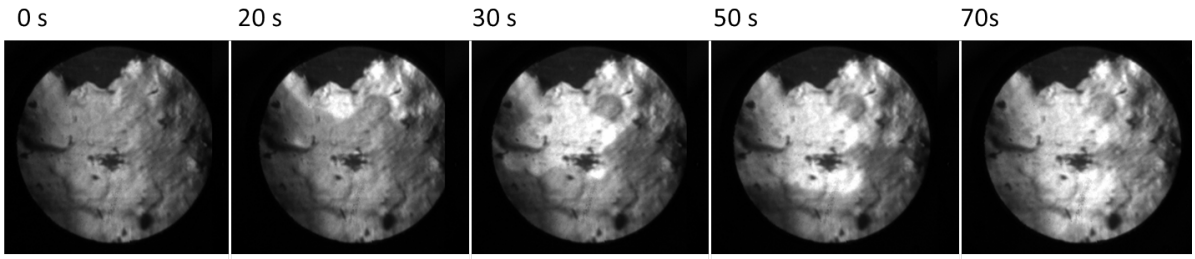

Fig. 4.5: PEEM video frames of the CO oxidation reaction on the Pd powder sample during the τ_B kinetic transition (p_{O_2}= 1.3×10^{-5} mbar, T= 180°C). The brightening of the surface means that the CO-covered Pd surface becomes oxygen-covered during the transition.

The main difference between the Pd black powder sample and a Pd foil lies within the surface morphology and amount of structural defects. These differences are reflected in the kinetic phase diagrams obtained for both the Pd powder and the Pd foil samples. It has to be noted, that for the Pd foil, two kinds of kinetic phase diagrams were determined in our laboratory, for an annealed and for an additionally sputtered surface [49]. The surface of a Pd foil after additional sputtering looks dramatically different than after smoothing of the defects by the annealing process, it disposes many steps and edges instead of relatively large terraces.

Let us first compare only the results for the annealed Pd foil and the same Pd foil after additional sputtering. Both kinetic transition points (τ_A and τ_B) for the sputtered Pd foil, are shifted towards higher CO pressures in respect to the transition points of the annealed surface. The shift of the transition points τ_A can be argumented by the higher adsorption energy for atomic oxygen at defect sites. The binding of CO to defect sites is also known to be stronger, but the increase is less significant than for oxygen. For the reverse transition

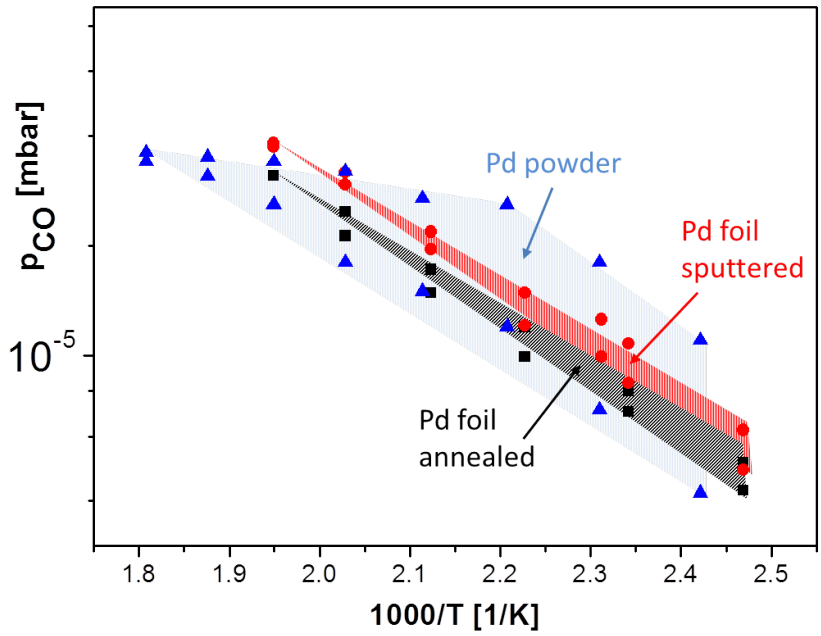

Fig. 4.6: Global kinetic phase diagram of a sputtered and annealed Pd foil taken from [49] compared with the global kinetic phase diagram of the supported Pd black powder

τ_B, the reactivation of the surface, a similar explanation can be applied: due to the high defect density, more adsorption sites for oxygen adsorption on a mainly CO-covered surface are available, the probability of oxygen adsorption is considerably higher and therefore, the reactivation occurs at a higher CO pressure on the defect-rich surface than on the annealed surface [49].

In turn, the comparison of the annealed and additionally sputtered Pd foils with the Pd powder shows (Fig.4.6), that the diagram for Pd powder is significantly wider than both of the foil-diagrams. The reason may lie in the fact, that the Pd powder particles consist of defect-rich regions, but can include also relatively smooth terraces. However this cannot explain such a wide diagram. Apparently the support-metal interaction contributes to the observed phenomena via enhanced adsorption of oxygen along the boundaries [50] or additional diffusion of CO (towards metal particles or towards support, depending on the temperature). Since present results are the first study in this direction, additional research is necessary to reveal the details of this complex interaction.

Nevertheless we can conclude from the comparison of the global kinetic diagrams for the Pd powder, annealed Pd foil and sputtered Pd foil, that with increasing concentration

of structural defects, the poisoning of the catalyst with CO coverage is shifted towards higher CO pressures and therefore a defect-rich catalyst is more tolerant against CO poisoning.

4.2 Palladium oxide in the CO oxidation

During the catalytic studies on metal surfaces the unavoidable question of the role of metal oxides and their activity arrises. In the case of palladium, few examples can be named, where palladium oxide has appeared to be the active phase. For example, PdO is active for catalytic combustion of methane at temperatures between 750-1000 K [51–54] and for oxidation of propene [55, 56].

Concerning the catalytic activity of PdO in respect to the CO oxidation, several groups claim, that the oxide phase formed under reaction conditions exhibits catalytic activity which is even higher than the the activity of a bare metal [57–60]. For example, Hendriksen et al. [57] suggests that the high reaction rate observed on oxidized Pd(100), is a result of the low stability of the oxide, making the surface highly reactive. It has been proposed that the CO oxidation on palladium oxide follows the Mars-Van Krevelen mechanism in which the oxide phase is continually consumed and reformed. Other authors, in turn, claim that the CO oxidation has a low reaction probability on metal oxides and explain this by the weak adsorption of CO on the oxide phase [61–67].

During oxidation of palladium different kind of oxides have been observed and excessively studied by many groups: a chemisorbed oxygen, Pd_5O_4 surface oxide, PdOx suboxide and bulk PdO [64, 68–74]. Their activity according to Gabasch et al.[64] could be summarized as follows. The most active phase is the chemisorbed oxygen on the metal surface, with the ability to coadsorb CO. The palladium surface oxide has been found active only due to growing metal-oxide phase boundaries. For bulk PdO, in turn, no activity has been observed below 493 K in respect to CO oxidation even around 10 mbar CO pressure due to lack of adsorption sites on this phase.

Despite the great effort made on this topic many details of the role of palladium oxide in the CO oxidation are still not clear. One of the issues of present thesis was to contribute to the clearing of this question by performing CO oxidation reaction kinetic measurements on a surface of palladium foil, which has been treated at oxygen pressures up to 10^{-6} mbar and elevated temperatures, and on PdO powder. Under conditions used in present study (p_{O_2} = 5×10^{-6} mbar, T = 400 - 700 °C) no PdO formation was observed on the Pd foil. Instead an impurity oxide has been formed as is presented in chapter 3. The results for the PdO powder are presented in chapter 4.2.3.

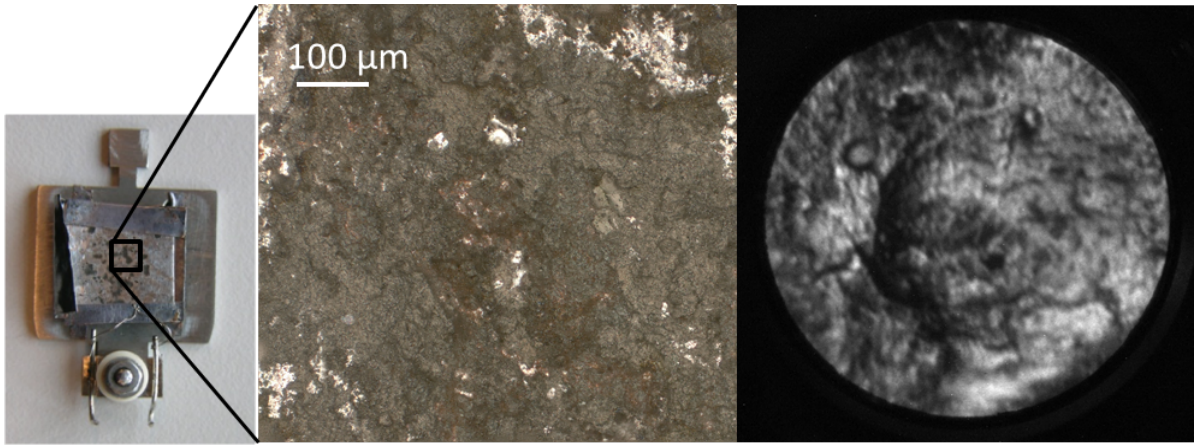

Fig. 4.7: a) The 10×10 mm "PdO powder on alumina" sample on the sample holder. b) Microscopic image of the same sample. c.) PEEM image of the same sample.

4.2.1 The PdO powder sample

The sample inspected in this chapter is palladium (II) oxide (Sigma Aldrich Inc., 99.998%) powder, which has been pressed into an aluminium foil, using a tantalum foil as a forcer. A 10×10 mm sample with the PdO powder has been fixed using tantalum frame onto a molybdenum sample holder, which can be locked with the transfer rod, so that the sample can be transferred from the "PEEM chamber" to the "XPS chamber" and *vice versa*.

4.2.2 Preparation of the PdO powder sample

Initial experiments with palladium oxide powder have shown, that sputtering and heating above 300°C leads to significant reduction of the oxide and also that there is carbon present on the surface, observed by XPS. In order to remove the carbon, the powder has been pretreated before being pressed into the foil with a flux of 50 ml/min oxygen-nitrogen mix (1:1) and a temperature ramp up to 500°C and held at this temperature for 2 and a half hours. Once inside the chamber, the sample has been treated under mild conditions to avoid reduction of the palladium oxide, i.e. the sample was only heated to temperatures between 200°C and 300°C in oxygen, namely at 1.3×10^{-5} mbar oxygen pressure for 15 minutes. For cleaning, the sample has been sputtered (argon pressure: $6{\times}10^{-6}$ to $8{\times}10^{-6}$ mbar, ion current of $\approx 2.5\mu$A and kinetic energy of 1 keV) for 15 minutes before each measurement.

4.2.3 Experimental results for PdO powder

Initial XPS measurements of the PdO sample, showed the palladium peaks $3d_{3/2}$ at 342.3 eV and $3d_{5/2}$ at 336.9 eV (Fig.4.8), which correspond to PdO (NIST database). However, after sputtering, heating and CO oxidation reaction, the XPS spectra usually showed maxima at values corresponding to the metallic palladium (Fig. 4.8) with a shoulder corresponding to PdO. That is, PdO can be reduced to a mixture of metallic Pd and PdO.

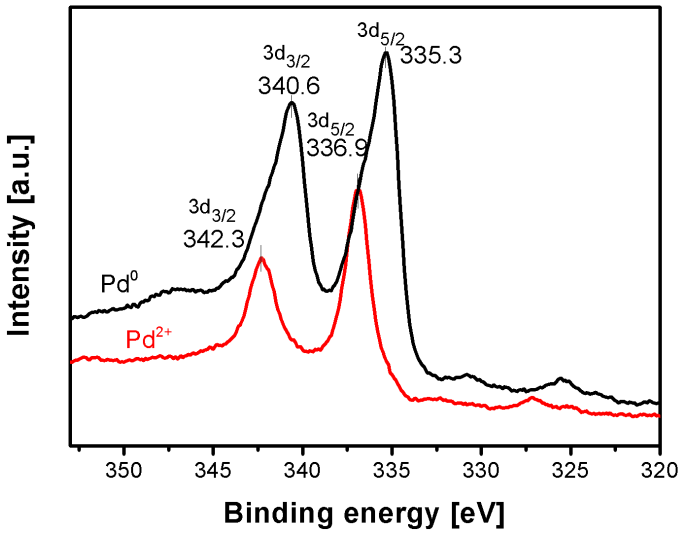

Fig. 4.8: Pd3d region in the XPS spectrum of the "PdO on alumina" sample; red: before cleaning and reaction; black: after sputtering, heating and CO oxidation reaction.

The CO oxidation reaction has been performed on the palladium oxide powder under the oxygen partial pressure of 1.3×10^{-5} mbar and constant temperature of 160 °C. Under these conditions and a CO pressure cycle, the hysteresis behavior of the CO oxidation could be observed. A measurement of the CO oxidation reaction by MS has also been performed without a sample in the chamber. MS measurements of the CO oxidation on the palladium oxide powder sample showed no activity in respect to the catalytic CO oxidation, shown by the overlap with the MS curve measured without a sample.

The XPS spectrum taken directly after the reaction showed palladium 3d peaks with maxima at the values known for palladium oxide and with a shoulder corresponding to Pd metal. The peak fitting has been performed using CasaXPS, whereas first a Shirley background has been subtracted from the spectrum and the line shape GL(90)T(1) has been used for the fits. GL(90) is a Gaussian-Lorentzian product function, where the mixing is 90% Lorentzian and 10% Gaussian function. Additionally the GL product function has been modified by the exponential blend (T).

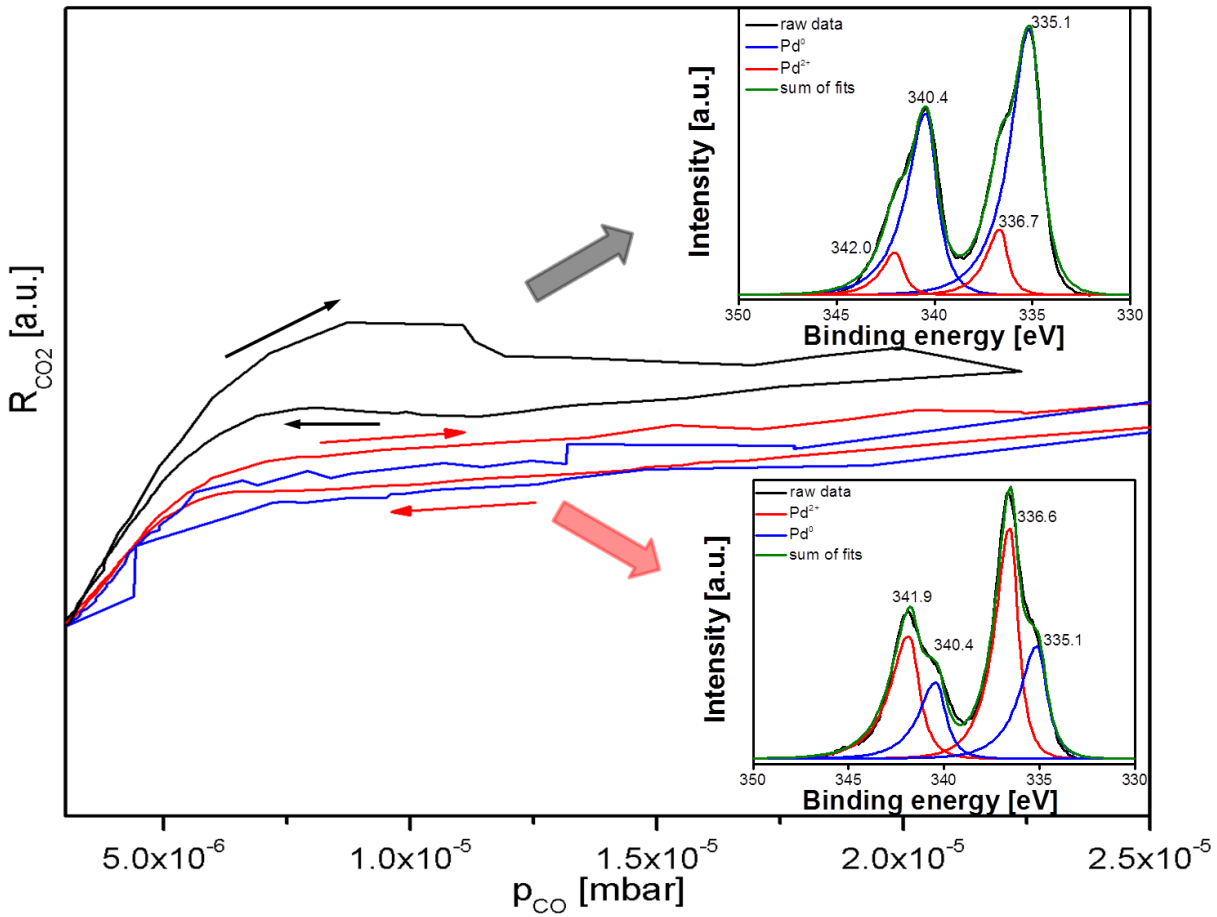

Fig. 4.9: CO_2 rate as a function of CO pressure followed by MS during the cyclic CO oxidation experiments. blue: MS measurement without a sample; red: MS measurement with the PdO sample; black: MS measurement with the PdO sample after partial reduction of the oxide by sputtering and exposure to the CO oxidation reaction conditions. The insets show corresponding XPS spectra obtained immediately after the reaction.

In the next step, the sample has been sputtered, as described in the Preparation section. This has led to an increase in the activity of the sample towards the CO oxidation as observed by the MS measurement (see Fig. 4.9). Consequent XPS measurements showed a mainly reduced palladium peak with a shoulder at the values known for PdO. This suggests the conclusion, that the increase in the activity came hand in hand with the reduction of the palladium oxide towards metallic palladium.

From the Fig. 4.9 one sees the overlapping MS-curve taken during the CO pressure cycle of the measurement with the empty chamber (blue) and with the PdO sample (red), giving a proof of the inactivity of the sample towards the catalytic CO oxidation. Directly after the CO oxidation reaction, the sample has been transfered to perform XPS measure-

ments. These have shown, that the sample consists of a mixture of Pd and PdO, in which PdO has the larger contribution. After repeating the cleaning procedure and the CO oxidation reaction on the sample, an increase in the activity has been observed and is seen in the Fig. 4.9 as the black MS-curve. The XPS measurement after this reaction has shown, that the PdO contribution in the sample at this point of the experiments is significantly lower than the metallic contribution.

4.3 Summary

In the first part of this chapter the study of the role of the surface morphology on the catalytic CO oxidation on palladium was presented. It has been done by determining a kinetic phase diagram for a palladium powder pressed onto an alumina support, used as a model catalyst and comparing it with the known kinetic phase diagrams of the annealed Pd foil and of the same foil after additional sputtering.

XPS measurements for the powder sample showed the presence of metallic palladium and mainly oxidized aluminium, which fulfilled the role of the support. Impurities, mainly carbon, have been minimized by surface cleaning in UHV under XPS control.

The combined MS, PEEM and XPS study of the Pd powder sample has been performed. Much higher PEEM intensity was observed for Pd powder sample than for the palladium foil, due to the significantly lower work function of a defect-rich Pd surface.

The CO oxidation on the supported Pd powder sample has been followed in the bistability region of the reaction by a cyclic CO pressure variation under isothermal conditions and constant oxygen pressure (p_{O_2}= 1.3×10^{-5} mbar). The transition points τ_A and τ_B for temperatures between 140 °C and 280 °C have been determined and used to construct an isothermal kinetic phase diagram, whereas the transition points, observed by the abrupt increase and decrease of the CO_2 rate in MS were used for the global kinetic measurements and the transition points determined by sudden darkening and brightening of the PEEM video were used for the local kinetic phase diagram.

In addition, "light-off" measurements have been performed in order to obtain the global kinetic phase diagram for isobaric conditions. During these experiments the CO and oxygen partial pressures were kept constant and the temperature was used as a variable external control parameter. The transition points of the "light-off" measurements were in agreement with the global kinetic phase diagram obtained under isothermal conditions.

The comparison of the global kinetic phase diagram of the supported powder with the kinetic phase diagram for an annealed and sputtered Pd foil has been performed. The

comparison shows, that the CO poisoning, i.e. kinetic transition to CO-covered surface (τ_A), occurs at higher CO pressures for defect-rich samples.

In the second part of the chapter results of studies of the activity of palladium oxide towards the catalytic CO oxidation on a PdO powder pressed into alumina support were presented. To remove carbon impurities, the powder has been pretreated with oxygen at elevated temperatures before entering the UHV system. This minimized the need of sample cleaning inside the UHV chamber and thus minimized reduction of the PdO towards metallic Pd. The XPS measurements of the powder sample have shown that the PdO is easily reduced at HV conditions and especially upon sputtering and heating without the presence of oxygen, apparently due to presence of CO in the rest gas atmosphere.

The CO oxidation reaction on the PdO sample has been followed by the PEEM and MS techniquea and a XPS spectrum has been recorded after each reaction cycle. The correlation between the metallic contribution and the activity in CO oxidation was observed: domination of PdO supresses the catalytic activity. Thus a conclusion can be made, that under present reaction conditions, metallic Pd and not PdO is the active phase in the CO oxidation reaction.

CHAPTER 5

SUMMARY AND CONCLUSIONS

In the present thesis the catalytic CO oxidation reaction on different palladium samples was studied *in situ* under HV reaction conditions by the MS, PEEM and XPS techniques. Different aspects affecting the CO oxidation have been investigated, such as formation of a thin silicon oxide layer originated from impurities segregating from the bulk, role of the surface morphology, and the contribution of the Pd oxide phase.

For kinetic measurements of the CO oxidation reaction the PEEM and MS techniques were implemented. In PEEM the contrast of the image is given by the variation of the work functions for different surface regions. Thus the transition from a brighter, oxygen-covered, to a darker, CO-covered, Pd surface during the CO oxidation reaction can be followed by PEEM. The intensity of the PEEM image has been integrated individually for different grains with low Miller indices during the reaction and plotted as a function of the CO pressure, thus determining the kinetic transitions locally for different (hkl) planes. The global kinetics were studied by MS, since with this technique the partial gas pressures inside the chamber can be determined and thus the reaction rate, CO_2 pressure, can be plotted as a function of the CO pressure.

The CO oxidation reaction was studied on a polycrystalline palladium foil, consisting of micrograins with individual (hkl) orientations, which enabled a simultaneous study of the catalytic behaviour of different (hkl) surfaces, exposed to the same reaction conditions. The reaction was studied in the oxygen partial pressure range of $\approx 10^{-5}$ mbar, CO partial pressure range between $\approx 10^{-6}$ - 10^{-5} mbar and the temperature of 160 °C. Under these conditions the reaction exhibited a bistable behaviour during an isothermal CO pressure cycle, as confirmed by a hysteresis observed both globally for the whole sample by MS and spatially-resolved for individual micrograins by PEEM.

The observed hysteresis consisted of a kinetic transition τ_A, from the initially oxygen-covered surface to the CO-covered surface and of the reversed transition τ_B, from the CO-covered to an oxygen-covered surface at remarkably lower CO pressure. The obtained hysteresis curve defines a region of bistability, where the surface of the catalyst can be either oxygen- or CO-covered, depending only on how these parameters have been reached, i.e. on the process prehistory.

During the oxidation of the Pd foil (at $\approx 10^{-6}$ mbar oxygen and at temperatures from 400°C to 700°C) a silicon oxide formation, caused by the oxygen assisted segregation of the silicon impurity to the Pd surface, has been detected. This effect and the role of the silicon oxide in the catalytic CO oxidation were studied in detail. The XPS measurements showed that with increasing oxidizing temperature, the concentration of silicon on the surface of the Pd foil has increased, thus silicon is more effectively segregating to the surface from the bulk. The chemical shift of the Si 2p peak by 3.4 eV to higher binding energies indicates that the silicon on the surface is immediately oxidized to SiO_2.

The effective activation energy for the process of segregation and oxide formation of the silicon has been determined from the Arrhenius plot to be 0.27 eV, i.e. a value, which is significantly smaller than known values for Si thermal oxidation, but somewhat larger than known values for plasma oxidation by atomic oxygen. This can be explained as follows: in our case adsorbed atomic oxygen is present on the palladium surface and therefore can be used for easier Si oxidation. The process is, in our case, limited by the segregation of Si from the bulk.

Kinetic measurements of the CO oxidation reaction for the palladium foil after its oxidizing treatment have shown, that the formation of SiO_2 on the surface of palladium significantly decreases its catalytic activity towards the CO oxidation reaction. The decrease in the activity parallels the increase of the amount of SiO_2 on the Pd surface.

A Pd powder sample supported by an oxidized aluminum foil has been studied in respect to CO oxidation in order to determine how the surface morphology affects the catalytic CO oxidation. The surface of the Pd powder particles, which were pressed into a foil has many more defect sites than a relatively smooth surface of the annealed Pd foil. Kinetic measurements of the CO oxidation reaction during the CO pressure cycle have been performed by PEEM and MS in the range of the hysteresis behavior (oxygen partial pressure of $\approx 10^{-5}$ mbar , CO partial pressure range between $\approx 10^{-6}$ - 10^{-5} mbar). The transition points as seen in PEEM have been used for the local kinetic phase diagram and the transition points as followed by MS for the global kinetic phase diagram. A kinetic phase diagram at temperatures between 140°C and 280°C has been constructed for the

Pd powder sample and compared with the kinetic phase diagrams of the Pd foil after annealing and of the same foil after additional sputtering.

Additionally "light-off" experiments under isobaric conditions and a temperature cycle have been performed. These experiments simulate the warming period of the motor engine after the "cold start", during which most of the pollutants are emitted. The catalytic converter becomes active after reaching its "ignition" temperature. The kinetic transition points obtained were in agreement with the phase diagram obtained for isothermal conditions. The comparison of the different phase diagrams allows a conclusion, that defect-rich surfaces are poisoned by CO coverage at higher CO pressure as a smooth surface. This can be explained by the higher adsorption energy for oxygen at defect sites.

Finally experiments on PdO powder pressed into an oxidized aluminum foil have been performed in order to shed light to the question about the role of palladium oxide in the catalytic CO oxidation. The control of the sample by XPS has shown that the PdO sample can be easily reduced by sputtering and heating in vacuum. The CO oxidation reaction on this sample has been performed at isothermal conditions (160 °C), partial oxygen pressure in the range of 10^{-5} mbar and a CO pressure cycle between $\approx 10^{-6}$ - 10^{-5} mbar has been carried out. The experimental results obtained under present reaction conditions showed that PdO appears to be inactive for the catalytic CO oxidation. Partial reduction of PdO to metallic Pd restores, at least partially, the catalytic activity.

LIST OF FIGURES

REFERENCES

[1] J.Hagen. *Industrial Catalysis.* Wiley-VCH., (2006).

[2] Thomas, J. and Thomas, W. *Principles and Practise of Heterogeneous Catalysis.* Wiley-VCH., (1997).

[3] Ostwald, W. *Phys. Z.* **3**, 313 (1902).

[4] Lindstrom, B. Pettersson, J. *CatTech* **7**, 130–138 (2003).

[5] Ertl, G. *Angew. Chem. Int. Ed.* **47**(19), 3524–3535 (2008).

[6] Jewel, L. and H.D., B. *Appl. Catal. A* **310**, 1–15 (2006).

[7] Wandelt, K. and Hulse, J. E. *J. Chem. Phys.* **80**, 1340 – 1352 (1984).

[8] Camara, G., Ticianelli, E., Mukerjee, S., Lee, S., and McBreen, J. *J. Electrochem. Soc.* **149**, A748–A753 (2002).

[9] Chorkendorff, I. and Niemandsverdriet, J. *Concepts of Modern Catalysis and Kinetics.* Wiley-VCH., (2003).

[10] Engel, T. and Ertl, G. *J. Chem. Phys.* **69**(3), 1267–1281 August (1978).

[11] Ertl, G., Neumann, M., and Streit, K. M. *Surf. Sci.* **64**(2), 393–410 May (1977).

[12] Norton, P. R., Davies, J. A., and Jackman, T. E. *Surf. Sci.* **122**(1), L593–L600 October (1982).

[13] Schlögl, F. *Z. Phys.* **248**, 446–458 (1971).

[14] Schlögl, F. *Z. Phys.* **253**, 147–161 (1972).

[15] Schlögl, F. *Ber. Bunsen-Ges. Phys. Chem.* **84**, 351–357 (1980).

[16] Boissonade, J. and de Kepper, P. *J. Phys. Chem.* **84**, 501 (1980).

[17] Burger, M. *Oscillations and Traveling Waves in Chemical Systems*. Wiley, (1985).

[18] Berdau, M., Karpowicz, A., Yelenin, G. G., Christmann, K., and Block, J. H. *J. Chem. Phys.* **106**(10), 4291–4308 (1997).

[19] Suchorski, Y., Imbihl, R., and Medvedev, V. K. *Surf. Sci.* **401**(3), 392–399 April (1998).

[20] Spiel, C. *PEEM microscopy and DFT calculations of catallytically active platinum surfaces and interfaces*. PhD thesis, Vienna University of Technology, (2012).

[21] Brueche, E. and Johannson, H. *Naturwissenschaften* **20**, 353–358 (1932).

[22] Hertz, H. *Ann. Phys.* **267**, 983–1000 (1887).

[23] Hallwachs, W. *Ann. Phys.* **269**, 301–312 (1888).

[24] Einstein, A. *Ann. Phys.* **322**, 132148 (1905).

[25] Smoluchowski, R. *Phys. Rev.* **60**, 661–674 (1941).

[26] Siegbahn, K., Nordling, C., and Lindberg, B. *ESCA: Atomic, Molecular, and Solid State Structure Studied by means of Electron Spectroscopy*. Almquist and Wiksells, (1967).

[27] Moulder, J., Stickle, W., Sobol, P., and Bomben, K. *Handbook of X-ray photoelectron spectroscopy*. Physical Electronics Inc., (1992).

[28] Auger, P. *J. Phys. Radium* **6**, 205–209 (1925).

[29] Seah, M. and Dench, W. *Surf. Interface Anal.* **1**, 2–11 (1979).

[30] Wagner, C. *Surf. Interface Anal.* **3**, 211 (1981).

[31] Over, H., Kim, Y., Seitsonen, A., Wendt, S., Lundgren, E., Schmid, M., Varga, P., Morgante, A., and Ertl, G. *Science* **287**, 1474–1476 (2000).

[32] Niehus, H. and Comsa, G. *Surf. Sci.* **102**(1), L14–L20 January (1981).

[33] Bader, S., Richter, L., and Orent, T. *Surf. Sci.* **115**(3), 501–512 March (1982).

[34] Gabasch, H., Knop-Gericke, A., Schlögl, R., Borasio, M., Weilach, C., Rupprechter, G., Penner, S., Jenewein, B., Hayek, K., and Klötzer, B. *Phys. Chem. Chem. Phys.* **9**, 533 – 540 (2006).

[35] Deal, B. E. and Grove, A. S. *J. Appl. Phys.* **36**, 3770–3778 (1965).

[36] Sekine, K., Saito, Y., Hirayama, M., and Ohmi, T. *IEEE T. Electron Dev.* **48**(8), 1550–1555 (2001).

[37] Saito, K., Jin, Y., T., O., and Shimada, M. *Jpn. J. Appl. Phys.* **43**, L765. (2004).

[38] Salmeron, M. and Somorjai, G. A. *J. Vac. Sci. Technol.* **19**, 722 – 725 (1981).

[39] Jones, R., Norton, L., Kramer, E., Bates, F., and Wiltzius, P. *Phys. Rev. Lett.* **66**, 1326 (1991).

[40] Binder, K. and P., F. *Spinodal Decomposition, in Phase Transformations in Materials.* Wiley-VCH., (2001).

[41] Aichmayer, B., Fratzl, P., Puri, S., and Saller, G. *Phys. Rev. Lett.* **91**, 015701 (2003).

[42] Hillert, M. *A Theory of Nucleation for Solid Metallic Solutions.* PhD thesis, MIT, (1955).

[43] Cahn, J. *Acta Met.* **9**, 795 (1961).

[44] Wandelt, K. *Surf. Sci.* **251/252**, 387–395 (1991).

[45] Knor, Z. *Surf. Sci.* **169**, L317–L320 (1986).

[46] Hopster, H., Ibach, H., and Comsa, G. *J. Catal.* **46**, 37–48 (1977).

[47] Lytken, O., Waltenburg, H., and Chorkendorff, I. *Surf. Sci.* **543**, 207–218 (2003).

[48] Ertl, G. *Catalytic Ammonia Synthesis Fundamentals and Practice.* Plenum, New York, (1991).

[49] Vogel, D., Spiel, C., Suchorski, Y., Stöger-Pollach, M., Schmid, M., Schlögl, R., and G., R. in preparation.

[50] Suchorski, Y., Wrobel, R., Becker, S., and Weiss, H. *J. Phys. Chem. C* **112**(50), 20012–20017 (2008).

[51] McCarty, J. *Catalysis Today* **26**, 283 (1995).

[52] Demoulin, O., Rupprechter, G., Seunier, I., Le Clef, B., Navez, M., and Ruiz, P. *Journal of Physical Chemistry B* **109**, 20454 (2005).

[53] Gabasch, H., Hayek, K., Klötzer, B., Unterberger, W., Kleimenov, E., and Teschner, D. *Journal of Physical Chemistry C* **111**, 7957 (2007).

[54] Ciuparu, D., Altman, E., and Pfefferle, L. *Journal of Catalysis* **203**, 64 (2001).

[55] Wang, J., Yun, Y., and Altman, E. I. *Surf. Sci.* **601**(16), 3497–3505 August (2007).

[56] Yun, Y., Wang, J., and Altman, E. *J. Catal.* **253**, 295 (2008).

[57] Hendriksen, B. L. M., Bobaru, S. C., and Frenken, J. W. M. *Surf. Sci.* **552**(1-3), 229–242 March (2004).

[58] Hendriksen, B. L. M., Bobaru, S. C., and Frenken, J. W. M. *Catal. Today* **105**(2), 234–243 July (2005).

[59] Rogal, J., Reuter, K., and Scheffler, M. *Phys. Rev. Lett.* **98**(4), 046101– January (2007).

[60] van Rijn, R., Balmes, O., Resta, A., Wermeille, D., Westerström, R., Gustafson, J., Felici, R., Lundgren, E., and Frenken, J. W. M. *Phys. Chem. Chem. Phys.* **13**(29), – (2011).

[61] Schalow, T., Brandt, B., Laurin, M., Schauermann, S., Libuda, J., and Freund, H.-J. *J. Catal.* **242**(1), 58–70 August (2006).

[62] Brandt, B., Schalow, T., Laurin, M., Schauermann, S., Libuda, J., and Freund, H.-J. *J. Phys. Chem. C* **111**(2), 938–949 January (2007).

[63] Schalow, T., Brandt, B., Laurin, M., Schauermann, S., Guimond, S., Kuhlenbeck, H., Libuda, J., and Freund, H.-J. *Surf.Sci.* **600**, 2528–2542 (2006).

[64] Gabasch, H., Unterberger, W., Hayek, K., Klötzer, B., Kresse, G., Klein, C., Schmid, M., and Varga, P. *Surf. Sci.* **600**(1), 205–218 January (2006).

[65] Gao, F., Wang, Y., Cai, Y., and Goodman, D. W. *J. Phys. Chem. C* **113**(1), 174–181 (2009).

[66] Chen, M. S., Cai, Y., Yan, Z., Gath, K. K., Axnanda, S., and Goodman, D. W. *Surf. Sci.* **601**(23), 5326–5331 December (2007).

[67] Zorn, K., Giorgio, S., Halwax, E., Henry, C. R., Grönbeck, H., and Rupprechter, G. *J. Phys. Chem. C* **115**, 1103–1111 (2011).

[68] Zemlyanov, D., Aszalos-Kiss, B., Kleimenov, E., Teschner, D., Zafeiratos, S., Hävecker, M., Knop-Gericke, A., Schlögl, R., Gabasch, H., Unterberger, W., Hayek, K., and Klötzer, B. *Surf. Sci.* **600**(5), 983–994 March (2006).

[69] Gabasch, H., Unterberger, W., Hayek, K., Klötzer, B., Kleimenov, E., Teschner, D., Zafeiratos, S., Hävecker, M., Knop-Gericke, A., Schlögl, R., Han, J., Ribeiro, F. H., Aszalos-Kiss, B., Curtin, T., and Zemlyanov, D. *Surf. Sci.* **600**(15), 2980–2989 August (2006).

[70] Zheng, G. and Altman, E. I. *Surf. Sci.* **462**(1-3), 151–168 August (2000).

[71] Zheng, G. and Altman, E. I. *Surf. Sci.* **504**, 253–270 April (2002).

[72] Voogt, E. H., Mens, A. J. M., Gijzeman, O. L. J., and Geus, J. W. *Surf. Sci.* **373**(2-3), 210–220 March (1997).

[73] Leisenberger, F. P., Koller, G., Sock, M., Surnev, S., Ramsey, M. G., Netzer, F. P., Klötzer, B., and Hayek, K. *Surf. Sci.* **445**(2-3), 380–393 January (2000).

[74] Todorova, M., Lundgren, E., Blum, V., Mikkelsen, A., Gray, S., Gustafson, J., Borg, M., Rogal, J., Reuter, K., Andersen, J. N., and Scheffler, M. *Surf. Sci.* **541**(1-3), 101–112 September (2003).

APPENDIX A

List of publications and oral presentations

1. D.Vogel, Z.Budinska, Y.Suchorski, C.Spiel, R.Schlögl, G.Rupprechter: "Silicon oxide surface segregation in CO oxidation on Pd: an in situ PEEM, MS and XPS study" Submitted to Applied Surface Science on 23.July 2012

2. Oral presentation on the 1st SFB FOXSI PhD-Seminar in Vienna, 11.May 2012: "Surface silicon oxide in CO oxidation on Pd: in situ PEEM and XPS-study"

APPENDIX B

This appendix includes a manuscript submitted to Applied Surface Science on 23. July 2012.

Submitted to Appl. Surf. Sci., on 23.July 2012

Silicon oxide surface segregation in CO oxidation on Pd: an in situ PEEM, MS and XPS study

D. Vogel[a,b], Z. Budinska[a], Y. Suchorski[a,*], C. Spiel[a], R. Schlögl[b], G. Rupprechter[a]

[a]*Institute of Materials Chemistry, Vienna University of Technology, Getreidemarkt 9, 1060 Vienna, Austria*

[b]*Fritz-Haber-Institut der Max-Planck-Gesellschaft, Faradayweg 4-6, 14195 Berlin, Germany*

**corresponding author, Tel.: +43 1 58801 165106, Fax: +43 1 58801 16599*

E-Mail address: yuri.suchorski@imc.tuwien.ac.at

Abstract

The effect of silicon oxide surface segregation on the locally-resolved kinetics of the CO oxidation reaction on individual grains of a polycrystalline Pd foil was studied in situ by PEEM, MS and XPS. The silicon oxide formation induced by Si-impurity segregation at oxidizing conditions, was monitored by XPS and its impact on the global and local (spatially-resolved) kinetics of the CO oxidation was determined by MS and PEEM. The results reveal a drastic inhibiting effect of silicon oxide on the Pd reactivity towards CO oxidation, manifested both in the collapse of the global CO_2 formation rate and in the modified local reactive properties of individual Pd micrograins. The presence of adsorbed oxygen on the Pd surface effectively enhances the silicon segregation to the Pd surface.

Keywords: CO oxidation, Pd, Si segregation, Si oxide formation, Photoemission electron microscopy, X-ray photoelectron spectroscopy

1. Introduction

Catalytic CO oxidation on Pt-group metal surfaces is often considered as a simple model reaction of significant practical meaning with respect to pollution emission control. More than three decades ago, pioneering molecular beam experiments of CO oxidation on Pd(111) surfaces performed by Engel and Ertl provided first evidence that the reaction follows the Langmuir-Hinshelwood mechanism [1]. Further applications of the surface science approach to single crystal surfaces revealed the elementary steps of this reaction such as molecular

adsorption of CO, dissociative adsorption of oxygen, surface reaction and desorption of carbon dioxide, and culminated in the Nobel Prize awarded to Gerhard Ertl in 2007 [2].

However, at the same time this seemingly simple model reaction was found to be quite complex in case of real catalysts consisting of oxide supported precious metal nanoparticles, and bridging the "materials and pressure gap" between the single crystal surfaces in UHV and real catalysts under ambient conditions is still a challenging task. To overcome the "material gap" between single crystal surfaces and real catalysts, many approaches have been applied, e.g. the investigation of field emitter tips [3], cylindrical single crystals [4] or polycrystalline foils [5-7]. A polycrystalline foil is a particularly suitable model system since it exhibits µm-sized domains of different orientations which are automatically exposed to exactly the same external parameters such as partial pressures and temperature. This means that precise comparative studies of the catalytic behavior of individual (hkl) orientations, such as the role of surface oxide formation can be performed, provided the applied experimental technique is able to read out the information from the µm-sized domains. Our new experimental approach based on PEEM (photoemission electron microscopy) exploits the parallel imaging principle of PEEM and uses the digital analysis of in situ recorded video-PEEM files allowing thus laterally resolved kinetic measurements on a µm-scale [7,8]. We have already applied this approach to study the local kinetics of the CO oxidation on individual grains of polycrystalline Pt [7,9], and Pd [10] foil and to directly compare the behavior of reaction-diffusion fronts on differently oriented domains [8,9].

New experimental developments of surface sensitive techniques applicable under high pressure conditions (i.e. mbar to atmospheric pressure), such as high-pressure STM (scanning tunnelling microscopy), PM-IRAS (polarization modulation infrared reflection absorption spectroscopy) and SFG (sum-frequency generation) have provided insights to catalytic reactions such as CO oxidation under more realistic catalytic conditions (bridging the "pressure gap" [11-16]). In some studies, (surface) oxide formation was observed in parallel with an activity increase and a Mars-van-Krevelen like mechanism has been proposed for the CO oxidation reaction on Pt and Pd surfaces at elevated pressures [16,17]. Despite an intensive debate about the nature of the most active phase in CO oxidation [18,19], the Langmuir-Hinshelwood mechanism still predicts well the kinetics of the CO oxidation reaction on Pt-group metals at both low and high pressures [12]: the O-covered surface responsible for the high catalytic activity in UHV, appears also as the most active phase at elevated pressures, unless oxide formation initiates the deactivation, especially for Pd and Rh surfaces.

Despite of the intensive studies of the role of palladium oxides in CO oxidation on Pd [20], much less attention is directed to the role of "non-palladium" oxides on the Pd surface in the CO oxidation. Recently it was shown, that such "stranger" oxides present on the platinum-metal surface, can significantly influence the reaction, even at small oxide coverages [21,22]. It is also known that impurities commonly present in commercially used catalysts, such as Si, might form surface oxides under oxidizing atmosphere [23], but, to our knowledge, aimed studies of such oxides under reaction conditions are very scarce. In the present contribution we apply PEEM combined with in situ XPS (x-ray photoelectron spectroscopy) and MS (mass-spectrometry) to study the role of the surface oxides formed by Si impurities in the kinetics of the CO oxidation on Pd.

2. Experimental

The experiments were performed in a UHV system consisting of two independently operated chambers connected with each other by a sample transfer line, thus allowing a common

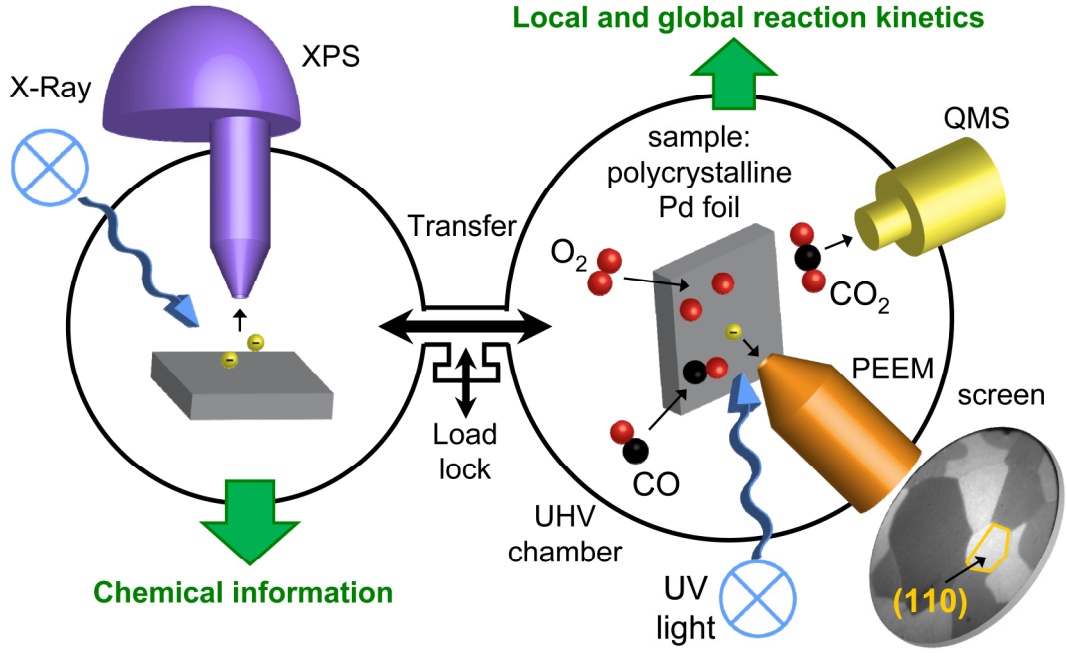

Fig. 1: Configuration of the experimental setup and scheme of the experiment. The simultaneous monitoring of the ongoing CO oxidation by PEEM and MS provides information on kinetic transitions on the whole sample (global MS measurements) and on the individual grains of a polycrystalline Pd foil (local PEEM measurements). The XPS analysis provides data on the chemical composition of the samples in UHV and under the same gas atmosphere as in PEEM.

reactive gas atmosphere in the 10^{-4} to 10^{-9} mbar range. The "microscopy" chamber is equipped with a PEEM (Staib Instruments), an MS (MKS Instruments), a LEED system (Omicron), a high purity gas supply system (O_2: 99.999%, CO: 99.97%) and sample preparation facilities for cleaning the sample by argon ion sputtering and subsequent annealing. The "spectroscopy" chamber is equipped with an XPS-system (Phoibos 100 hemispherical energy analyzer and XR 50 twin anode X-ray source, SPECS). The general configuration of the experimental setup and a scheme of the experiment are shown in Fig. 1.

The investigated sample, a 10x10 mm^2 polycrystalline Pd foil (AlfaAesar, 99.9% purity), consists mainly of [100]-, [110]- and [111]-oriented grains which were formed after annealing the foil for several hours at 1100 K in UHV. The sample temperature was measured by a NiCr/Ni thermocouple spot-welded to the front side of the Pd sample. Prior to catalytic measurements, the surface was Ar^+ sputtered and annealed at 1073 K.

The principle of the local kinetic measurements by PEEM has been described in detail before [7-9] and is therefore summarized here only briefly (see also Fig. 1). The CO oxidation reaction on the Pd foil is monitored simultaneously by MS and by PEEM, whereby MS provides the global CO_2 rate produced by the whole polycrystalline sample. PEEM, in turn, provides the laterally-resolved kinetic information from the individual grains.

The PEEM image which is formed by photoelectrons created by UV light illumination of the sample (with a deuterium discharge lamp, E_{max} ~ 6.5 eV) reflects the lateral distribution of the local work function across the sample. This allows for differentiation between grains of different surface orientation and between different adsorbates by correlation of the local image intensity with the work function values of the corresponding clean and adsorbate-covered single crystals [7]. The PEEM-image is recorded in situ with a high-speed CCD-camera (Hamamatsu), so the intensity of a selected region-of-interest, i.e. one particular grain, can be monitored during a typical CO pressure scan. The XPS analysis provides data on the chemical composition of the samples in UHV or under the same gas atmosphere as in PEEM.

3. Results and discussion

3.1 Global and local reaction kinetics

To correlate the kinetic transitions in CO oxidation reaction on individual grains on the polycrystalline Pd foil with the averaged (global) kinetics of the whole sample, the orientation of the individual grains was established first, and global kinetic studies in the bistability range of CO oxidation were performed. The results are summarized in Fig. 2: the upper row (Fig. 2a-c) shows PEEM-frames of the clean (Ar^+ sputtered and annealed) Pd foil (Fig. 2a), the

same surface covered by adsorbed oxygen (Fig. 2b) and again the same area but after oxygen treatment at 973 K and $5x10^{-6}$ mbar (Fig. 2c). In Fig. 2a three individual [110]-, [100]- and [111]-oriented grains are indicated, whose crystallographic orientation has been determined by the differences in contrast, as described in detail in Ref. [7]. The lower plots in Fig. 2 show the global (MS-measured for the whole sample) CO_2 reaction rate recorded during an isothermal cyclic CO pressure scan at constant oxygen pressure of $1.3x10^{-5}$ mbar for the clean, i.e. sputtered and annealed Pd surface (Fig. 2d), and for the same surface which was additionally treated by oxygen at $p_{O2} = 5x10^{-6}$ mbar for 15 min at three different temperatures of 873 K, 973 K and 1073 K, also in comparison with the clean Pd surface (Fig. 2e). Typically for CO oxidation on Pd, the surface in the high reactivity steady state (predominantly oxygen-covered), exhibits an almost linear increase of the CO_2 production rate with increasing CO pressure, till a kinetic transition from the high reactivity state to a low reactivity state occurs (Fig. 2d). This is the result of the collapsing oxygen adsorption due to the CO-induced poisoning (inhibition of dissociative oxygen adsorption, [2]) of the Pd surface. The corresponding transition point is termed τ_A whereas the point of the reverse transition is called τ_B (Fig. 2d).

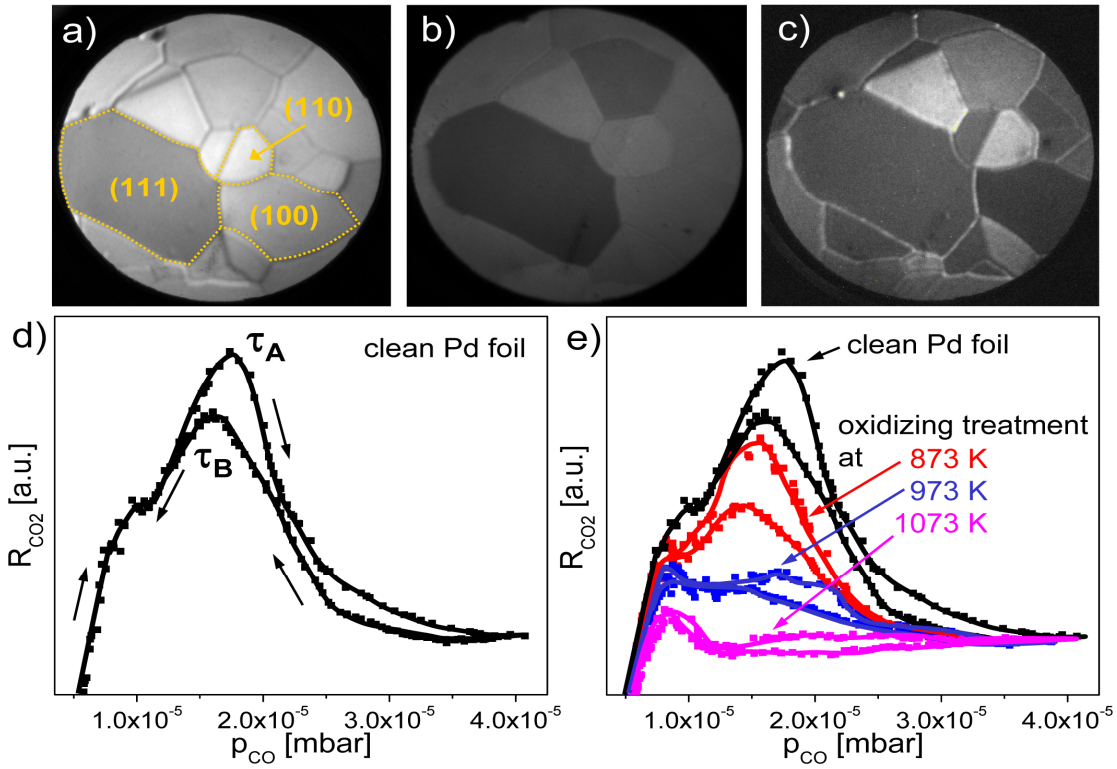

Fig. 2: CO oxidation on polycrystalline Pd foil. (a) PEEM image of the clean (Ar^+ sputtered and annealed) Pd surface, three low index domains are exemplary indicated; (b) the same surface, but oxygen covered; (c) the same surface after oxidizing treatment at $p_{O2} = 5x10^{-6}$ mbar and T = 973 K; (d)

global CO_2 reaction rate for a clean Pd surface recorded by MS during an isothermal (T = 473 K) cyclic CO pressure scan at constant oxygen pressure of $1.3x10^{-5}$ mbar. Kinetic transitions τ_A and τ_B from the catalytically active to the inactive steady state and vice versa are indicated; (e) the same as in (d) but for the oxygen treated surface ($p_{O2} = 5x10^{-6}$ mbar, T = 873 K; 973 K; 1073 K, treatment duration 15 min for all temperatures). A CO_2 reaction rate curve for the clean surface is also shown for comparison.

Because of the effective blocking of adsorption sites for oxygen by CO the reverse transition τ_B from the inactive to the active state occurs at a lower CO partial pressure than the transition τ_A, resulting in the hysteresis in CO_2 production rate as seen in Fig. 2d for the sputtered and annealed Pd surface and in Fig. 2e for the Pd surface treated at 873 K in oxygen at $5x10^{-6}$ mbar. Such hysteresis-like behavior of the CO oxidation reaction is called bistability since two states of the reaction system are possible at the same parameter set depending on the system's prehistory (for details see refs. [21,22]).

For the Pd surface treated by oxygen at 873 K the CO_2 rate appears considerably lower, but the hysteresis is still present (Fig. 2e). Oxygen treatment at higher temperatures causes further decrease of the CO_2 rate (e.g. for 973 K, Fig. 2e) and even a disappearance of the hysteresis (see the 1073 K curve in Fig. 2e).

For the laterally resolved kinetics of the CO oxidation, the video-PEEM sequences (recorded simultaneously with the MS monitoring) were analyzed. Figure 3a shows an example of such analysis where the *local* PEEM intensity for a particular domain, in the present case a Pd(110) domain, is shown in analogy to the *globally* MS-measured CO_2 rate in Fig. 2d. The local data result in a clear hysteresis where two sharp drops/jumps of the PEEM intensity are visible. Analogue to the changes in the overall CO_2 reaction rate in dependence of the CO partial pressure as measured by MS, the drops/jumps in the PEEM intensity represent kinetic transitions from one reactivity state of the system to another, but measured locally for one particular grain of interest. The reason for the much more pronounced local transitions observed by PEEM (in comparison to MS) lies in the averaging effect of the MS measurements: the kinetic transitions of the differently oriented grains occur at different CO pressures, the corresponding drops/jumps in the R_{CO2} curve overlap, thus smearing out the global τ_A and τ_B.

Again, similarly as in the global case, the treatment of the polycrystalline Pd surface with oxygen at elevated temperature (e.g. at 973 K as is shown in Fig. 3b) results in the collapse of the hysteresis loop, the local τ_A and τ_B transitions are smeared out and it is not possible to associate the transitions with particular CO pressure values as in the case of the clean Pd

surface (Fig. 3a). The reason for this behavior will be discussed below, together with the XPS data.

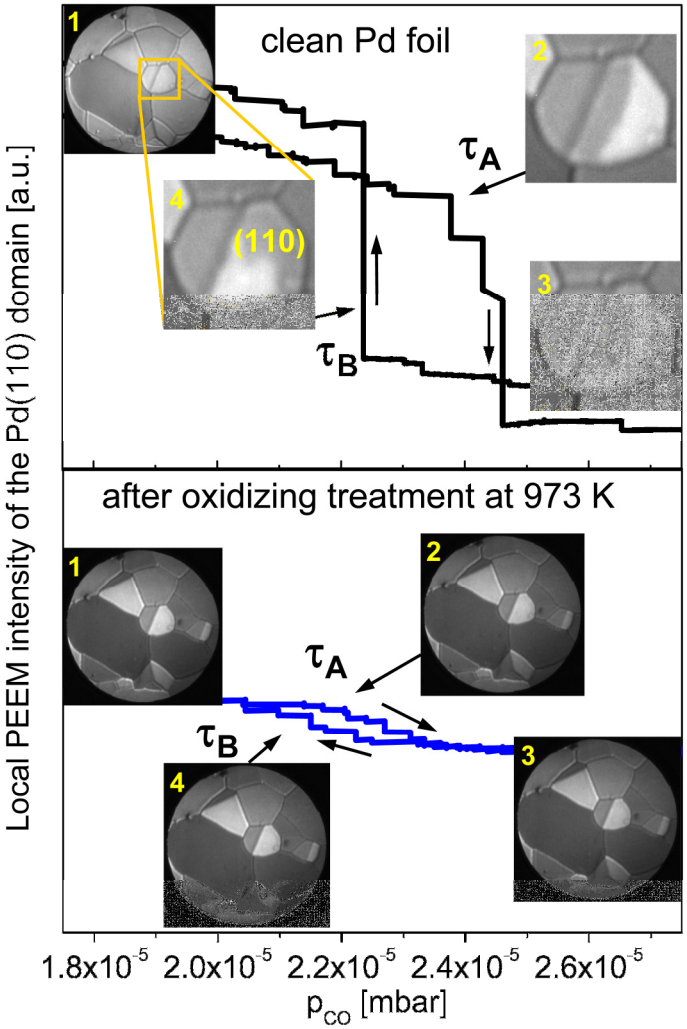

Fig. 3: Laterally-resolved kinetics of CO oxidation on individual grains of the Pd foil.
(a) local intensity of the PEEM image for the Pd(110) domain recorded during the same cyclic CO pressure scan as in Fig. 2d. The kinetic transitions τ_A and τ_B are much more pronounced than in the global MS curve (Fig. 2d). The PEEM frames correspond to the reaction stages indicated in the PEEM intensity curve; (b) the same as in (a) but after the oxidizing oxygen treatment at 973 K. The τ_A and τ_B points are almost indiscernible.

3.2 XPS results

To explain the observed reaction behavior, an XPS-analysis of the Pd foil has been performed before and after the oxidizing oxygen treatment at constant oxygen pressure of $5x10^{-6}$ mbar and temperatures between 673 K and 973 K. The XPS results are summarized in Figs. 4a-c, in which the high-resolution spectra for the Pd 3d region (Fig. 4a), for the Si 2p region (Fig. 4b) and the evolution of the Si 2p signal with surface oxidation temperature (Fig. 4c) are shown.

The Pd 3d spectra demonstrate that no significant formation of palladium oxide has been observed under the present conditions. In turn, the Si 2p spectra reveal a remarkable SiO_2 formation on the Pd surface upon the oxidizing treatment at elevated temperatures. Apparently, the presence of oxygen stimulates the diffusion of bulk dissolved Si from the near-surface regions towards the surface and thus enhances the segregation of Si to the Pd surface (compare the Si^0 and the Si^{4+} 2p signals, measured for the Si segregated without and with oxygen atmosphere). As for any diffusion related process, the segregation limited SiO_2 formation rate appears to be strongly temperature dependent, as demonstrated in Fig. 4c. An attempt to apply an Arrhenius plot provides an effective activation energy of 0.27 eV, a value which is significantly lower than known values of about 2 eV for thermal Si oxidation [24,25]. It is clear, however, that in the present case of a submonolayer SiO_2, the Deal-Grove model [24] based on the assumption that Si oxidation proceeds by the transport of molecular oxygen from the ambient to the Si/SiO_2 interface through already oxidized Si layers does not apply. In our case, the rate limitation does not result from the oxygen diffusion, but from the silicon transport from the Pd subsurface region to the surface. Thus, the activation energy values typical for the oxygen diffusion limited process are not expected. Recently, unusually small activation energy values (of e.g. 0.13 eV [25] or even lower [26]) were observed for the oxidation procedure where the oxygen diffusion limit was lifted by using atomic oxygen for Si oxidation.

Generally, experimental observations are known, which show that the presence of oxygen (even in the 10^{-6} mbar range) increases the mobility of Si in Pt-metals causing the precipitation of SiO_x at the surface [27]. The enhanced Si segregation in the presence of oxygen can be rationalized considering energetic arguments: the higher bonding strength of Si on an oxygen covered Pd surface provides an energetic sink for Si atoms due to the chemical potential gradient, similarly as it occurs e.g. in an enrichment of alkali atoms on the oxygen covered surface in CO oxidation on Rh [28] or hydrogen oxidation on Rh [29,30], or in the formation of concentration patterns of electropositive adsorbates as a result of up-hill diffusion in two-dimensional first order phase transitions under reaction-free conditions [31,32]. Recently, DFT calculations were performed to identify the stable Si-O bonding structures on the Pd(111) and Pt(111) surfaces [33], where a variety of stable intermediates with stoichiometries between SiO_2 and SiO_3, depending on the coverage, were found. This might explain the inhibiting effect of the SiO_x growth on the PdO_x formation observed in the present experiments, again due to the energetic arguments which favor the Si rather than the Pd oxidation.

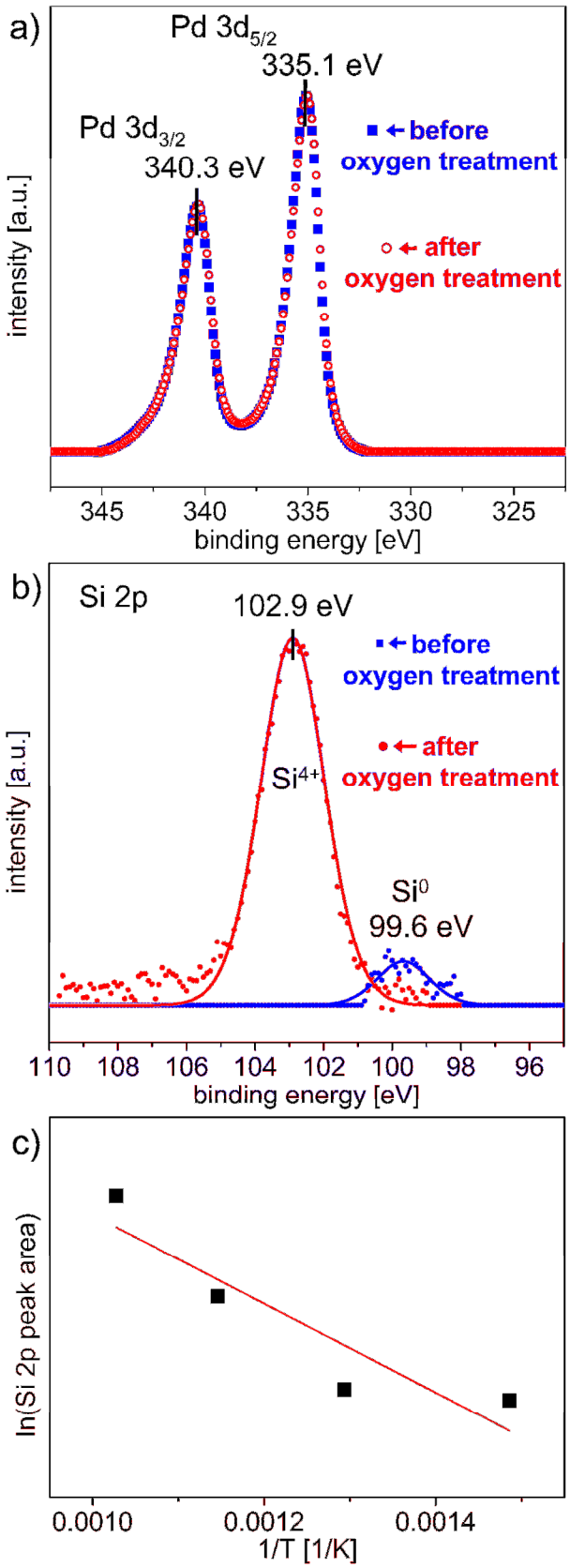

Fig. 4: Silicon oxide formation on Pd surface: a) Pd 3d XPS spectra before and after oxidizing oxygen treatment at 973 K; b) the same but for the Si 2p spectra; c) Arrhenius plot.

The easiest interpretation of the inhibiting role of SiO_2 in the CO oxidation reaction would be that SiO_2 simply blocks a part of the active reaction sites on the Pd surface but does itself not participate in the reaction. However, the drastic decrease in the CO_2 formation rate for a rather small coverage of SiO_2 (just a fraction of a monolayer, as follows from the Pd 3d and Si 2p signal relation) requires an additional explanation. It is known that oxides on the Pt-group metals form monolayer islands at the initial growth stage [22,34]. The boundary lines between the oxide islands and the remaining "oxide-free" metal surfaces exhibit, due to the local electron density jump from the metal to the oxide surface, different electronic properties which may nanometer-wide extend the promoting effect along the free metal surface around the islands [22].

The promoting effect on the reaction observed in the case of CeO_x islands, which is due to the additional oxygen supply [22], cannot be expected for SiO_2 because of the poor redox properties of SiO_2 and thus the absence of an oxygen storage capacity. Whereas the refilling of the oxygen vacancies in reducible oxides such as CeO_x stimulates the oxygen dissociation on the oxide-island adjacent surface sites, this is not the case for SiO_2. In turn, the spillover of CO from the SiO_2 islands (a weakly bound mobile CO layer can be formed on the SiO_2 surface [35]) supports the interpretation that the regions around the SiO_2 islands must be rather inactive for the CO oxidation.

4. Summary

A combined PEEM-MS-XPS approach allows us to study the in situ kinetics of surface reactions under control of the surface chemical composition of the sample, also under reactive atmospheric conditions in the 10^{-5} mbar range. This also allows to trace reaction induced compositional changes of the sample surface, e.g. as the result of segregation effects.

In the present study silicon oxide formation, resulting from Si-impurity segregation on the polycrystalline Pd-foil at oxidizing conditions in the temperature range between 873 K and 1073 K, was monitored by XPS and its impact on the global and local (spatially-resolved) kinetics of the CO oxidation was determined by MS and PEEM. The results reveal a drastic inhibiting effect of silicon oxide on the Pd reactivity towards CO oxidation, manifested both in the collapse of the global CO_2 formation rate (as measured by MS) and in the modified local reactive properties (as observed by PEEM) of individual Pd micrograins. The presence of adsorbed oxygen on the Pd surface effectively enhances the silicon segregation to the Pd surface, due to energetic reasons.

Acknowledgements

Technical support by Johannes Frank (IMC, TU Vienna) is cordially acknowledged. This work was partially supported by the Austrian Science Fund (FWF) [SFB-F45-04 FOXSI] and by the ÖAD, Project 84ÖU5.

References

[1] T. Engel, G. Ertl, J. Chem. Phys. 69 (1978) 1267.

[2] G. Ertl, Angew. Chem. Int. Ed. 47 (2008) 3524, and references therein.

[3] Y. Suchorski, W. Drachsel, Top. Catal. 46 (2007) 201, and references therein.

[4] M. Sander, R. Imbihl, G. Ertl, J. Chem. Phys. 97 (1992) 5193.

[5] J. Lauterbach, G. Haas, H.H. Rotermund, G. Ertl, Surf. Sci. 294 (1993) 116.

[6] J. Lauterbach, H.H. Rotermund, Catal. Lett. 27 (1994) 27.

[7] Y. Suchorski, C. Spiel, D. Vogel, W. Drachsel, R. Schlögl, G. Rupprechter, ChemPhysChem 11 (2010) 3231, and supporting information.

[8] D. Vogel, C. Spiel, Y. Suchorski, A. Urich, R. Schlögl, G. Rupprechter, Surf. Sci. 605 (2011) 1999.

[9] C. Spiel, D. Vogel, Y. Suchorski, W. Drachsel, R. Schlögl, G. Rupprechter, Catal. Lett. 141 (2011) 625.

[10] D.Vogel, C. Spiel, Y. Suchorski, A. Trinchero, H. Grönbeck, R. Schlögl, G. Rupprechter, (2012) submitted to Angew. Chem. Int. Ed.

[11] D.W. Goodman, C.H.F. Peden, M.S. Chen, Surf. Sci. 601 (2007) L124.

[12] F. Gao, Y. Wang, Y. Cai, D.W. Goodman, J. Phys. Chem. C 113 (2009) 174.

[13] F. Gao, Y. Cai, K K. Gath, Y. Wang, M.S. Chen, Q.L. Guo, D.W. Goodman, J. Phys. Chem. C 113 (2009) 182.

[14] F. Gao, S.M. McClure, Y. Cai, K.K. Gath, Y. Wang, M.S. Chen, Q.L. Guo, D.W. Goodman, Surf. Sci. 603 (2009) 65.

[15] G. Rupprechter, C. Weilach, J. Phys.: Condens. Matter 20 (2008) 184019.

[16] B.L M. Hendriksen, J.W.M. Frenken, Phys. Rev. Lett. 89 (2002) 046101.

[17] B.L.M. Hendriksen, S.C. Bobaru, J.W.M. Frenken, Surf. Sci. 552 (2004) 229.

[18] R. van Rijn, O. Balmes, R. Felici, J. Gustafson, D. Wermeille, R. Westerström, E. Lundgren, J.W.M. Frenken, J. Phys. Chem. C 114 (2010) 6875.

[19] F. Gao, Y. Wang, D.W. Goodman, J. Phys. Chem. C 114 (2010) 6874.

[20] K. Zorn, S. Giorgio, E. Halwax, C.R. Henry, H. Grönbeck, G. Rupprechter, J. Phys. Chem. C 115 (2011) 1103.

[21] Y. Suchorski, R. Wrobel, S. Becker, B. Strzelczyk, W. Drachsel, H. Weiss, Surf. Sci. 601 (2007) 4843.

[22] Y. Suchorski, R. Wrobel, S. Becker, H. Weiss, J. Phys. Chem. C 112 (2008) 20012.

[23] S. Bader, L. Richter, T. Orent, Surf. Sci. 115 (1982) 501.

[24] B.E. Deal, A.S. Grove, J. Appl. Phys. 36 (1965) 3770.

[25] K. Sekine, Y. Saito, M. Hirayama, T. Ohmi, IEEE Trans. Electr. Dev. 48 (2001) 1550.

[26] K. Saito, Y. Jin, T. Ono and M. Shimada, Jpn. J. Appl. Phys. 43 (2004) L765.

[27] M. Salmeron, G.A. Somorjai, J.Vac.Sci.Techn. 19 (1981) 722.

[28] Y. Suchorski and J.H. Block, Appl.Surf. Sci. 94/95 (1996) 200.

[29] H. Marbach, S. Günther, B. Luerssen, L. Gregoratti, M. Kiskinova, R. Imbihl, Catal. Lett. 83 (2002) 161.

[30] H. Marbach, G. Lilienkamp, H. Wei, S. Günther, Y. Suchorski, R. Imbihl, Phys. Chem. Chem. Phys. 5 (2003) 2730.

[31] A.G. Naumovets, in: D.A. King, D.P. Woodruff (Eds.), The Chemical Physics of Solid Surfaces, vol. 7, Elsevier, Amsterdam, 1994, p. 163.

[32] I. Lyuksyutov, A.G. Naumovets, V. Pokrovsky, Two-Dimensional Crystals, Academic Press, Boston, 1992.

[33] D.C. Kershner, M.P. Hyman, J.W. Medlin, Surf. Sci. 602 (2008) 3603.

[34] C. Klein, G. Kresse, S. Surnev, F.P. Netzer, M. Schmid, P. Varga, Phys. Rev. B 68 (2003) 235416.

[35] A. Blomqvist, L. Lehman, P. Salo, Phys. Stat. Sol. 249 (2012) 1046